inorganics

MDPI

Review

Research Progress of Halide Perovskite Nanocrystals in Biomedical Applications: A Review

Guiyun Wang [1,†], Yanxia Qi [1,†], Zhiyan Zhou [2,*], Zhuang Liu [3] and Ruowei Wang [1,*]

[1] College of Nursing, Shandong Xiehe University, Jinan 250109, China
[2] School of Stomatology, Cheeloo College of Medicine, Shandong University & Shandong Key Laboratory of Oral Tissue Regeneration & Shandong Engineering Research Center of Dental Materials and Oral Tissue Regeneration & Shandong Provincial Clinical Research Center for Oral Diseases, Jinan 250012, China
[3] School of Materials Science and Engineering, Shandong University, Jinan 250061, China; liu.zhuang@sdu.edu.cn
* Correspondence: zhouzhiyan@sdu.edu.cn (Z.Z.); wangruowei@sdxiehe.edu.cn (R.W.)
† These authors contributed equally to this work.

Abstract: Halide perovskite nanocrystals have rapidly emerged as a prominent research topic in materials science over the past decade owing to their exceptional optoelectronic properties and tunability. Their distinctive characteristics, including high light absorption coefficients, high quantum yields, narrow-band emissions, low defect densities, and adjustable chemical compositions and sizes, position them as highly promising candidates for applications in optoelectronic devices, energy conversion units, and other related systems. However, due to the toxicity and instability of halide perovskite nanocrystals, their widespread application in the biomedical field has been limited in the past. In recent years, numerous innovative coating strategies have been reported to effectively enhance the stability of halide perovskite nanocrystals while confining their toxic metal ions within the coating layers, thereby significantly improving their biocompatibility. This review provides a comprehensive summary of the recent progress of halide perovskite nanocrystals in the field of biomedicine. It covers coating strategies to enhance stability and biocompatibility, as well as the applications of coated halide perovskite nanocrystals in biomedicine, with a particular focus on their unique advantages in bioimaging and chemical sensing. Finally, we address unresolved issues and challenges, such as the metabolic pathways and final products of halide perovskite nanocrystals in vivo. We hope to inspire researchers in the field and provide direction for future studies.

Keywords: halide perovskite nanocrystal; coating; stability; biocompatibility; biomedical application; bioimaging; chemical sensing

check for updates

Academic Editors: Sake Wang, Nguyen Tuan Hung and Minglei Sun

Received: 17 January 2025
Revised: 11 February 2025
Accepted: 11 February 2025
Published: 13 February 2025

Citation: Wang, G.; Qi, Y.; Zhou, Z.; Liu, Z.; Wang, R. Research Progress of Halide Perovskite Nanocrystals in Biomedical Applications: A Review. *Inorganics* **2025**, *13*, 55. https://doi.org/10.3390/inorganics13020055

Copyright: © 2025 by the authors. Licensee MDPI, Basel, Switzerland. This article is an open access article distributed under the terms and conditions of the Creative Commons Attribution (CC BY) license (https://creativecommons.org/licenses/by/4.0/).

1. Introduction

Halide perovskite nanocrystals, characterized by the ABX_3 crystal structure, consist of an organic or inorganic cation at the A site (e.g., methylamine MA^+ or Cs^+), a divalent metal cation at the B site (e.g., Pb^{2+} or Sn^{2+}), and halide anions (e.g., Cl^-, Br^-, or I^-) occupying the X site [1–3]. Over the past decade, these nanomaterials have emerged as a cornerstone in materials science, attributed to their outstanding optoelectronic properties and exceptional versatility [4,5]. Their distinctive features—including superior light absorption coefficients, impressive quantum efficiencies, sharp emission spectra, minimal defect states, and customizable chemical and morphological attributes—position them as promising candidates for a wide array of applications, ranging from advanced optoelectronic devices and energy harvesting systems to scintillator technologies and beyond [6–10].

1.1. Advantages of Halide Perovskite Nanocrystals and Their Applications

The remarkable light absorption capacity and luminescence efficiency of halide perovskite nanocrystals make them highly advantageous for optoelectronic applications [11,12]. With photoluminescence quantum yields (PLQY) approaching nearly 100% and exceptionally narrow emission bandwidths (commonly exhibiting a full width at half maximum, FWHM, of less than 25 nm), they deliver unparalleled color purity [13,14]. Moreover, the emission wavelength can be precisely controlled across the visible spectrum and extended into the near-infrared (NIR) region by fine-tuning the nanocrystals' chemical composition and size [15–17]. The synthesis of halide perovskite nanocrystals is relatively simple and encompasses scalable techniques, such as solution-phase methods and hot-injection protocols [18–21]. These methods typically enable large-scale production under mild conditions, ensuring cost-effectiveness and adaptability for diverse application scenarios. Additionally, the morphologies of halide perovskite nanocrystals can be engineered with great flexibility, spanning zero-dimensional (0D) quantum dots, one-dimensional (1D) nanowires, two-dimensional (2D) nanosheets, and three-dimensional (3D) bulk crystals [22–26]. This structural versatility significantly expands their applicability across various domains. Beyond their exceptional optical attributes, halide perovskite nanocrystals demonstrate excellent charge carrier mobility (20–100 $cm^2\ V^{-1}\ s^{-1}$) and extended carrier diffusion lengths (1–10 μm) [27–29]. These properties further enhance their performance in optoelectronic devices and energy-related technologies, cementing their status as transformative materials in modern science and engineering.

Halide perovskite nanocrystals have gained widespread recognition for their diverse applications across multiple fields. Notably, they have shown tremendous promise in solar cells, light-emitting diodes (LEDs), photodetectors, and lasers [30–32]. For instance, perovskite quantum dot-based LEDs, celebrated for their exceptional color purity and tunable spectral output, are emerging as transformative components in display technologies [33–35]. Similarly, perovskite photodetectors, characterized by broad spectral sensitivity and high detection efficiency, have proven invaluable for advancements in communication and imaging systems [36–38]. The utilization of halide perovskite nanocrystals is also expanding into photocatalysis [39,40]. Recent studies highlight their superior catalytic performance in critical reactions, including water splitting for hydrogen generation, carbon dioxide reduction, and the degradation of organic pollutants [41–43]. Beyond optoelectronic and catalytic domains, halide perovskite nanocrystals are increasingly recognized for their potential in energy storage technologies, paving the way for novel solutions in renewable energy systems [44–46]. However, compared to other semiconductor materials, such as small-molecule organic dyes, which have already been widely utilized in the biomedical field, the application of halide perovskite nanocrystals in this domain appears to be in its nascent stages.

1.2. Biotoxicity and Instability of Halide Perovskite Nanocrystals

Although halide perovskite nanocrystals exhibit remarkable optical and electronic properties that position them as promising candidates for medical applications, their biotoxicity and inherent instability remain significant barriers to their widespread adoption in biomedical fields and clinical practice [47]. The biotoxicity of perovskite nanocrystals is largely attributed to their chemical composition, particularly the presence of Pb^{2+} ions [48]. While Pb^{2+} contributes to the superior optoelectronic performance of certain perovskite materials, its accumulation in biological systems poses severe risks, including cellular and organ damage (Figure 1) [49,50]. Extensive studies have demonstrated that Pb^{2+} ions exhibit toxic effects, potentially causing neurotoxicity, liver and kidney impairment, immune suppression, and reproductive dysfunction [51]. During biomedical applications, if the lead

content in perovskite nanocrystals is not adequately controlled or encapsulated, Pb^{2+} may be released into the body, triggering adverse biological responses and increasing long-term health risks [52]. Moreover, the nanoscale dimensions of perovskite nanocrystals allow them to penetrate cell membranes with ease, interacting with intracellular biomolecules [53]. This interaction can result in oxidative stress, deoxyribonucleic acid (DNA) damage, and apoptosis. Additionally, the biocompatibility of perovskite nanocrystals can be influenced by surface defects and surface passivation strategies, potentially leading to cytotoxicity and immune responses [54]. These challenges underscore the critical need for innovative approaches to mitigate the biotoxicity and enhance the stability of halide perovskite nanocrystals for their safe application in biomedical fields.

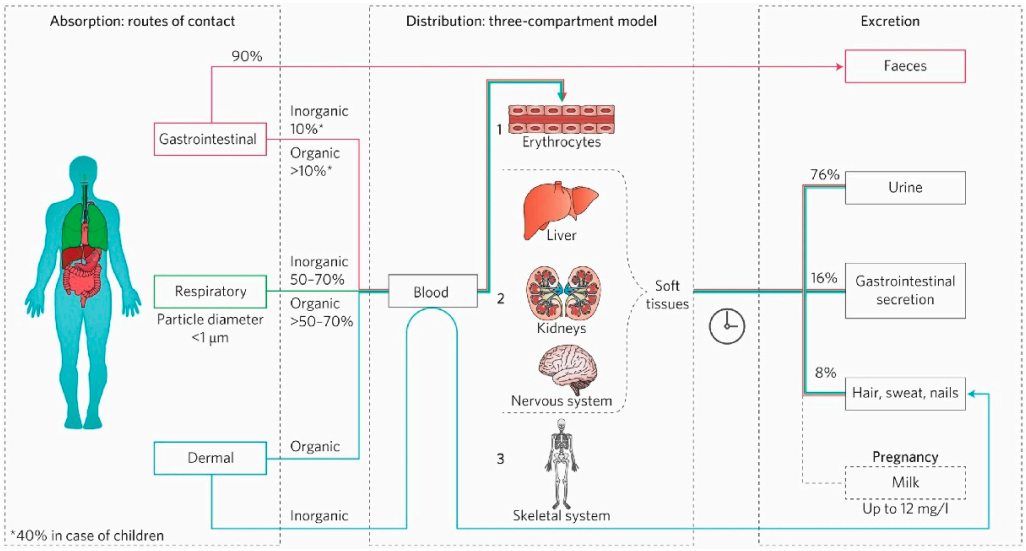

Figure 1. A schematic illustration depicting the absorption, distribution, and excretion pathways of lead compounds within the human body. For each exposure route, the percentage indicates the proportion of lead absorbed. Lead not absorbed through gastrointestinal ingestion is expelled via feces, while unabsorbed lead from respiratory or dermal exposure is presumed to be exhaled or removed through natural bodily processes, respectively. Once absorbed, lead accumulates in three primary compartments of the body, where it is retained for durations specific to each organ before eventual excretion. Reprinted with permission from ref. [49]. Copyright 2016, Springer Nature.

Furthermore, lead leakage from perovskite materials into the soil can be absorbed by plants and subsequently enter the food chain at rates up to ten times higher than other lead contaminants introduced through human activities, thereby posing severe biological toxicity risks (Figure 2) [55]. Experimental findings underscore the necessity of the meticulous handling of lead from halide perovskites. Notably, it has been emphasized that the permissible lead content in perovskite-based materials must be significantly lower than that in other lead-containing electronic devices. Consequently, researchers strongly advocate for the complete substitution of lead with more inert and environmentally benign metals to facilitate the safe advancement of perovskite technologies.

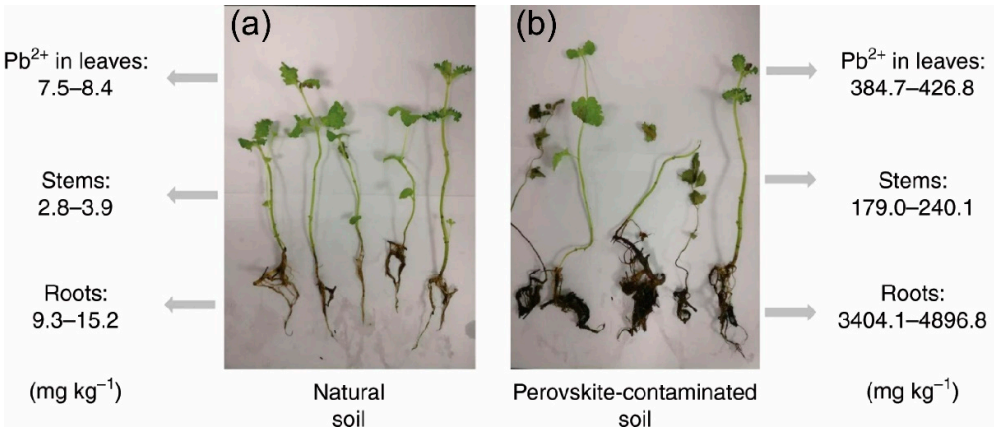

Figure 2. The image illustrates mint plants cultivated in (**a**) uncontaminated control soil and (**b**) soil contaminated with Pb^{2+} from perovskite materials. The lead concentrations detected in the leaves, stems, and roots are displayed adjacent to each corresponding section of the plants. Reprinted with permission from ref. [55]. Copyright 2020, Springer Nature.

A major limitation of perovskite materials is their poor chemical and environmental stability [56–58]. Halide perovskite nanocrystals are highly susceptible to degradation when exposed to humidity, oxygen, ultraviolet (UV) light, and heat, challenges that are particularly pronounced in the complex environment of the human body. This instability leads to significant performance deterioration over time, restricting their potential for biomedical applications. Moisture sensitivity is one of the primary factors compromising the stability of halide perovskites [59]. Exposure to moisture can degrade their crystal structure, causing optical performance to decline or even leading to complete crystal dissociation. Within biological environments, the presence of both moisture and oxygen exacerbates this degradation, further limiting their durability for applications like biological imaging and therapeutic interventions. Additionally, halide perovskite nanocrystals are prone to structural and functional degradation under UV light and elevated temperatures [60,61]. This is particularly problematic for biomedical uses, such as in vivo or in vitro photothermal therapy (PTT), where exposure to UV light and heat is often unavoidable [62–64].

Surface defects further compromise the stability of halide perovskites [65,66]. The high surface energy of these materials makes them susceptible to degradation, especially in the presence of water or oxygen. Such defects not only degrade the optical performance of the material but may also induce cytotoxic responses in biological systems. Addressing these stability challenges is crucial for advancing the safe and effective use of halide perovskite nanocrystals in biomedical fields.

1.3. Current Solutions to Address Biotoxicity and Instability

To address the challenges outlined above, current research focuses on several key strategies. To mitigate the toxicity associated with lead, significant efforts have been directed toward developing lead-free perovskite materials, such as substituting tin (Sn^{2+}) for lead [67,68]. These lead-free alternatives effectively reduce toxicity risks. However, studies have shown that exposure to SnI_2 can be more acutely toxic to zebrafish than PbI_2, with toxicity levels closely correlated to the pH of the growth medium (Figure 3) [49]. Additionally, despite their reduced toxicity, lead-free halide perovskites face persistent challenges, including limited stability and lower luminescence efficiency, highlighting the need for continued optimization to enhance their practical viability [16,69].

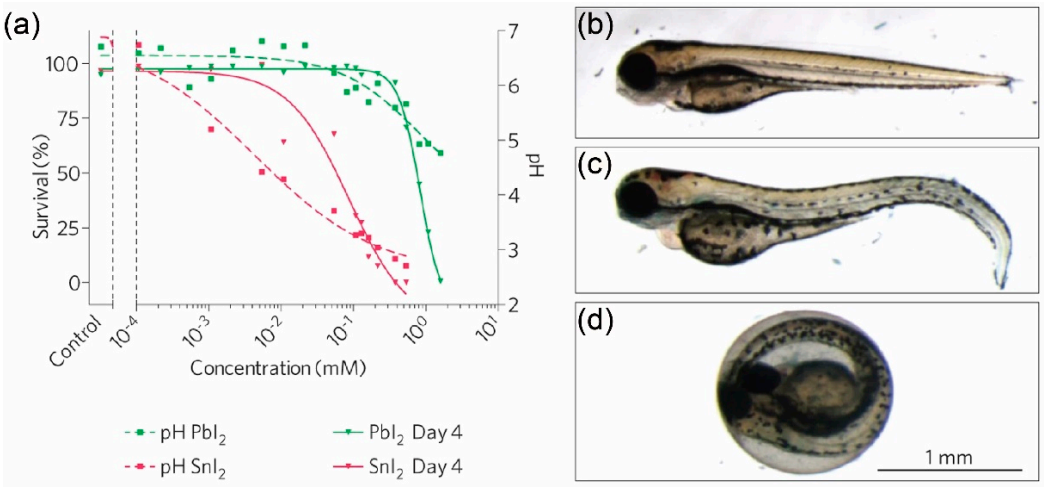

Figure 3. (**a**) Survival rate of zebrafish, 4 days post-fertilization, plotted against toxicant concentration and pH. (**b**) Healthy zebrafish (control group). (**c**) Zebrafish exposed to PbI_2, displaying brain hemovascular defects, heart edema, and dorsal curvature. (**d**) Zebrafish embryo exposed to SnI_2, exhibiting failure to hatch at 96 h post-fertilization. Reprinted with permission from ref. [49]. Copyright 2016, Springer Nature.

Surface modification and encapsulation techniques offer effective solutions to enhance the biocompatibility and chemical stability of perovskite nanocrystals [8,70,71]. As early as around thirty years ago, studies had already reported that halide perovskite $(C_6H_5C_2H_4NH_3)_2PbI_4$ encapsulated in polymethyl methacrylate (PMMA) polymers could be fabricated on SiO_2 substrates by performing spin-coating and subsequent annealing processes [72,73]. The as-prepared halide perovskite compounds were dispersed as nanometer-sized crystals, and, more importantly, their stability was considerably improved. Similar strategies have been in use up to the present day. For example, coating halide perovskite nanocrystals with organic or inorganic materials—such as polymers or silica—can isolate toxic components and reduce moisture and oxygen infiltration, thereby significantly improving their stability [74,75]. Furthermore, surface modifications can further bolster the in vivo stability of halide perovskite nanocrystals, ensuring they retain exceptional performance over extended periods of use.

Simultaneously, to guarantee the long-term stability of perovskite nanocrystals in biomedical applications, it is crucial to establish a robust stability assessment system. This system should encompass a thorough evaluation of their degradation rate, long-term stability, and biotoxicity within the in vivo environment. Such an assessment framework will provide the scientific evidence necessary to support the clinical translation of these materials.

This review provides a comprehensive overview of the research advancements in halide perovskite nanocrystals within the biomedical field, building upon the background discussed. It covers strategies for enhancing the stability of halide perovskite nanocrystals, application cases in biological imaging, and their use in environmental monitoring and biosensing. We believe that this review not only highlights the significant progress made in these areas but also serves as a source of inspiration for further research in the biological sciences, thereby fostering the continued exploration of halide perovskite nanocrystals in the biomedical domain.

2. Halide Perovskite Nanocrystals for Bioimaging Applications

Halide perovskite materials inherently suffer from reduced stability in aqueous environments and exhibit even greater instability in complex biological settings. To overcome this limitation, halide perovskite nanocrystals must be encapsulated within protective

matrices [76]. Currently, two primary strategies are employed to enhance the water stability of halide perovskite nanocrystals: (i) surface coating of individual nanocrystals and (ii) encapsulation of multiple nanocrystals within water-resistant matrices [77,78]. The surface coating approach involves applying water-protective shells, such as silica or titanium dioxide, directly onto individual perovskite nanocrystals. Alternatively, encapsulation techniques embed multiple perovskite nanocrystals within robust matrices made from polymers or phospholipids, effectively shielding them from water exposure.

For bioimaging applications, the challenge becomes even more complex, as halide perovskite nanocrystals often interact directly with biological environments, including blood, cells, and tissues—highly intricate aqueous systems composed of ions, salts, proteins, and other biomolecules. Consequently, the protective coatings for halide perovskite nanocrystals must not only be water-resistant but also demonstrate exceptional stability in biological fluids to ensure their functionality and reliability in biomedical applications. Despite recent progress in using halide perovskite nanocrystals as imaging tags for living cells, the in vivo stability remains largely unproven, representing a significant challenge for clinical translation [79].

A recent study has introduced a universal approach aimed at advancing the potential bioimaging applications of halide perovskites [80]. Specifically, researchers have proposed an effective method for encapsulating $CsPbBr_3$ halide perovskite nanocrystals within organized microscale polymer carriers, rendering them water-resistant (Figure 4a,b). Following the comprehensive structural and optical characterization of the resulting materials, their stabilities in various biological fluids, including phosphate-buffered saline and human serum, and within a cellular microenvironment (CT26 cells) were evaluated. For the first time, the in vivo stability of encapsulated halide perovskite nanocrystals was assessed using Dilute Brown Non-Agouti (DBA) mice (Figure 4c). Cell–halide perovskite nanocrystal interactions were visualized using confocal laser scanning microscopy, with cell membranes being stained red and cell nuclei being stained blue. The bright green fluorescence emitted by the halide perovskite nanocrystals highlighted the water-resistant properties of the organic polymer coating, demonstrating its stability in an aqueous biological environment (Figure 4d).

To assess the in vivo stability of $CsPbBr_3$ nanocrystals encapsulated in polymer microscale carriers, the carriers were intramuscularly injected into DBA mice. Following injection, the mice were euthanized, and their tissues were collected and prepared for histological analysis using fluorescent staining. The results showed bright fluorescence from the nanocrystals exclusively in the muscle tissue, with no detectable fluorescence in other tissues (Figure 4e). This finding indicates that the microscale carriers containing halide perovskite nanocrystals remained localized at the injection site without dispersing to other tissues. Notably, the encapsulated nanocrystals retained their fluorescence for up to 72 h post-injection, highlighting the durability of the polymer coating even under in vivo conditions. Compared to highly efficient commercial up-conversion nanoparticles doped with rare-earth ions, halide perovskite nanocrystals offer significant advantages in both cost and performance [81–83]. The fabrication of halide perovskite nanocrystals is approximately one tenth the cost of up-conversion nanoparticles, and they exhibit a much broader excitation spectral range, thereby enhancing their versatility for a wide range of applications. Thus, the encapsulation strategy developed in this study presents a promising pathway for utilizing halide perovskite nanocrystals as stable fluorescence tags in bioimaging, ensuring both durability and functionality in complex biological environments.

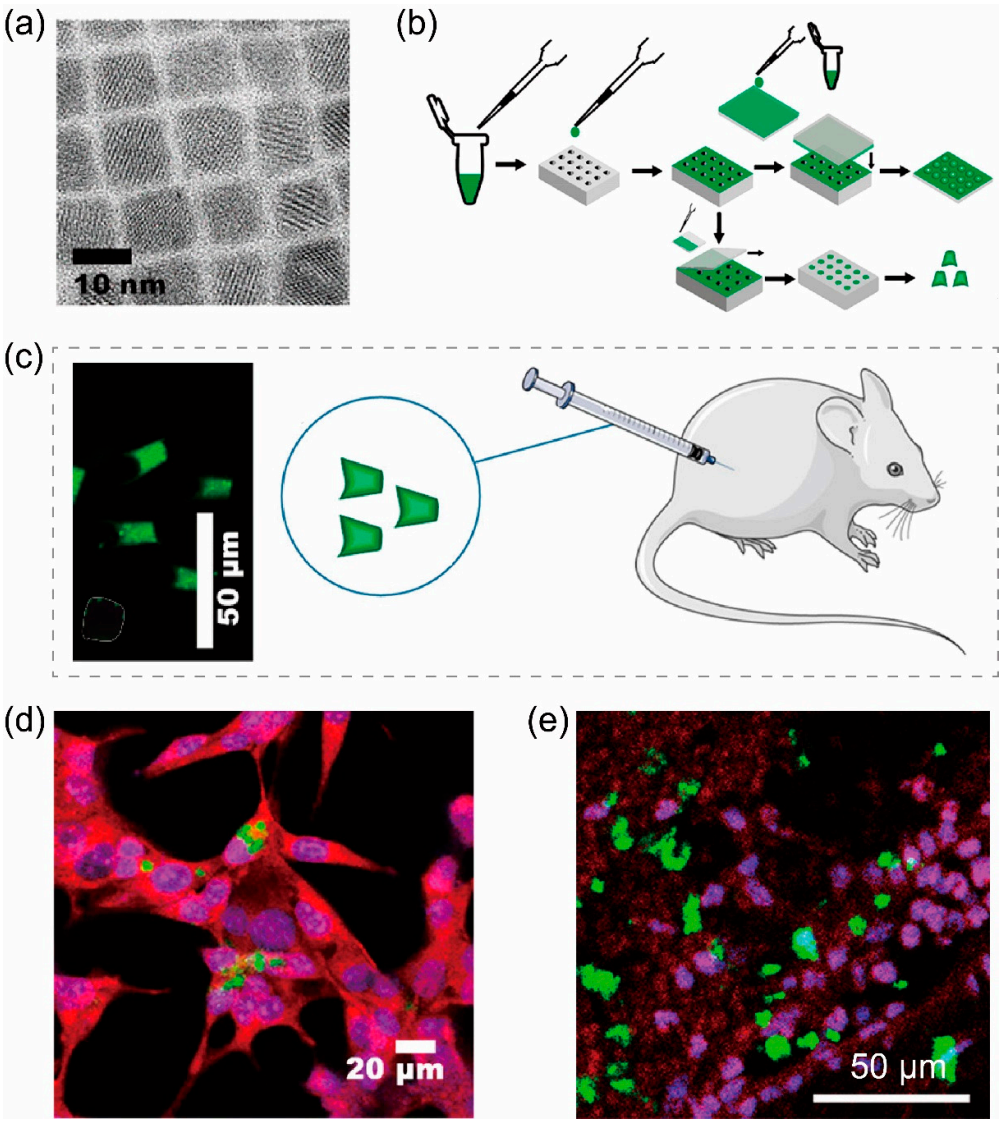

Figure 4. (**a**) High-resolution transmission electron microscopy (HRTEM) image of $CsPbBr_3$ nanocrystals. (**b**) Schematic illustration depicting the fabrication strategies for microscale carriers loaded with $CsPbBr_3$ nanocrystals. (**c**) Confocal laser scanning microscopy image of microscale carriers loaded with $CsPbBr_3$ nanocrystals. (**d**) Confocal laser scanning microscopy image of CT-26 cells incubated with microscale carriers containing $CsPbBr_3$ nanocrystals for 24 h. (**e**) Confocal laser scanning microscopy image of muscle tissue following intramuscular injection of microscale carriers loaded with $CsPbBr_3$ nanocrystals. Reprinted with permission from ref. [80]. Copyright 2022, American Chemical Society.

Composite particles, such as the aforementioned microscale carriers, are too large to be efficiently internalized into the cytoplasm, limiting their suitability for small-cell imaging applications [84,85]. In a recent study, insoluble $CsPbBr_3/CsPb_2Br_5$ composite nanocrystals were successfully synthesized through a simple water-assisted chemical transformation of halide perovskite nanocrystals (Figure 5a) [86]. Water plays two critical roles in this process: (i) it removes CsBr from $CsPbBr_3/Cs_4PbBr_6$, and (ii) it alters the coordination number of Pb^{2+}, changing it from six in $CsPbBr_3$ and Cs_4PbBr_6 to eight in $CsPb_2Br_5$. Figure 5b shows photographs of $CsPbBr_3/CsPb_2Br_5$ composite nanocrystals dispersed in toluene and water under UV light (365 nm), where the composite nanocrystals emit bright green fluorescence in both solvents. Remarkably, the water-dispersed $CsPbBr_3/CsPb_2Br_5$ composite nanocrystals exhibit exceptional photoluminescent (PL) properties, maintaining

a high PLQY of 80% and a narrow FWHM of 16 nm. These characteristics closely resemble those of the original $CsPbBr_3/CsPb_2Br_5$ nanocrystals (PLQY of 83%) and pure $CsPbBr_3$ nanocrystals dispersed in toluene (PLQY of approximately 90%). These properties position $CsPbBr_3/CsPb_2Br_5$ composite nanocrystals as highly effective fluorescent probes for live HeLa cell imaging.

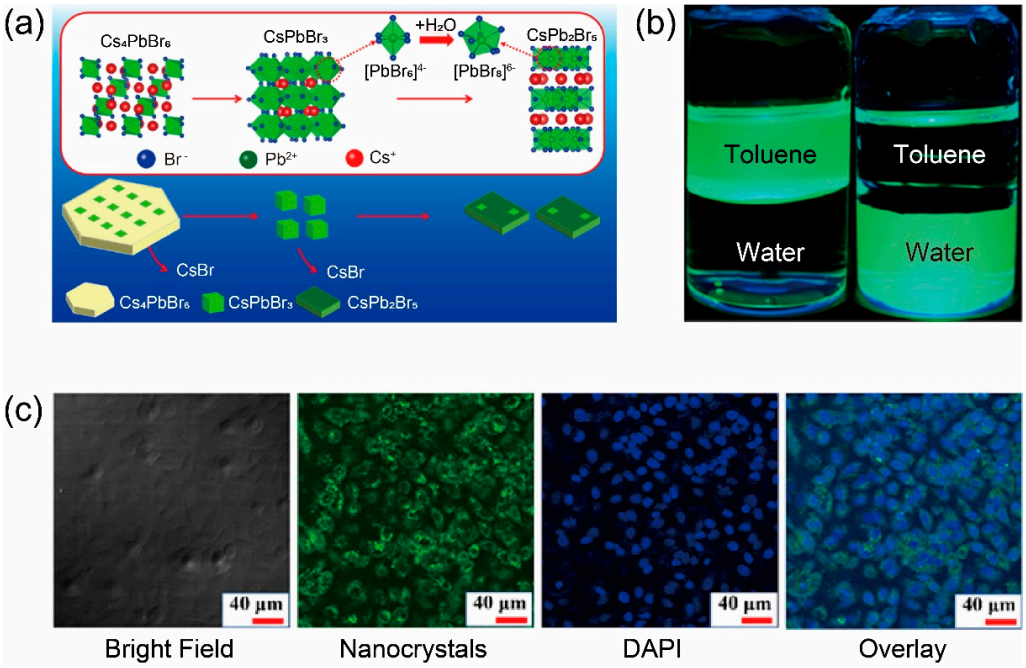

Figure 5. (**a**) Schematic diagram illustrating the water-assisted transformation process, which depicts the conversion of $CsPbBr_3/Cs_4PbBr_6$ composite nanocrystals into $CsPbBr_3/CsPb_2Br_5$ composite nanocrystals. (**b**) Photographs showcasing $CsPbBr_3/CsPb_2Br_5$ composite nanocrystals dispersed in toluene and water taken under UV light (365 nm). (**c**) Bright-field and fluorescence images of HeLa cells incubated with $CsPbBr_3/CsPb_2Br_5$ nanocrystals for 24 h, with nuclei stained in blue using 4,6-diamidino-2-phenylindole (DAPI) dye. The overlay images reveal the cellular uptake of the nanocrystals. Reprinted with permission from ref. [86]. Copyright 2019, American Chemical Society.

High water stability is a critical requirement for the effective application of $CsPbBr_3/CsPb_2Br_5$ composite nanocrystals in cell imaging. The potentials of the as-prepared $CsPbBr_3/CsPb_2Br_5$ composite nanocrystals for cellular imaging were further explored. As shown in Figure 5c, fluorescence images of HeLa cells incubated at 37 °C with $CsPbBr_3/CsPb_2Br_5$ composite nanocrystals for 24 h reveal green fluorescence localized around the nucleus. This observation confirms that the composite nanocrystals successfully penetrate the cell membranes and enter the cells. In contrast, larger $CsPbBr_3$ nanocrystals encapsulated in polystyrene ($CsPbBr_3$@PS) have been previously used as cellular labeling agents [87]. However, the luminescence intensities of the labeled cells decreased with extended incubation times. The differences in performance between $CsPbBr_3$@PS and $CsPbBr_3/CsPb_2Br_5$ composite nanocrystals could be attributed to two factors. First, a larger quantity of $CsPbBr_3/CsPb_2Br_5$ composite nanocrystals was internalized into the cytoplasm due to their nanoscale size, which differed from the processes that the larger $CsPbBr_3$@PS particles underwent. Second, the $CsPbBr_3/CsPb_2Br_5$ nanocrystals exhibited highly stable luminescence in aqueous solutions. Therefore, this study not only introduces a novel method for preparing insoluble, narrow-band, and brightly luminescent composite nanocrystals but also broadens the potential applications of halide perovskite nanocrystals in biomedicine.

Despite the presence of an effective protective coating, the fluorescence intensity of halide perovskite nanocrystals inevitably diminishes over time due to inherent defects, leading to a deterioration in performance [88–90]. For instance, the fluorescence intensity of the encapsulated halide perovskite nanocrystals, as depicted in Figures 4 and 5, significantly declines after just one week, rendering them unsuitable for prolonged bioimaging applications [80,86]. Consequently, researchers are investigating methods to extend the fluorescence longevity of halide perovskite nanocrystals. A recent study introduced an innovative, stepwise approach for encapsulating $CsPbBr_3$ nanocrystals within water-soluble polymer capsules [91]. This adaptable protocol accommodates nanocrystals with diverse surface ligands. Notably, the encapsulated nanocrystals exhibit a remarkable PLQY of approximately 60%, which remains stable for over two years when the capsules are dispersed in water. The capsule fabrication process is illustrated in Figure 6a, while Figure 6b,c showcase images of the capsules in water under UV light. These capsule solutions display a milky dispersion and emit vibrant green fluorescence upon UV exposure. Remarkably, this fluorescence persists for several months. A representative TEM image reveals the formation of well-defined, spherical capsules. Within these capsules, both aggregated and individual nanocrystals are present, with the latter situated at the core and surrounded by a polymer shell approximately 25-nm thick (Figure 6d).

Following encapsulation and redispersion in water, researchers selected a batch of samples exhibiting high PLQY. These samples were stored in sealed vials at room temperature, with their PLQY monitored over a two-year period. Figure 6e depicts the temporal evolution of the sample's PLQY. The protocol employed in this study demonstrated exceptional efficacy in preventing water infiltration through the hydrophobic regions of the polymer. Consequently, the capsules maintained their emission profile and PLQY while dispersed in water, with the Cs–oleate and DDAB-coated $CsPbBr_3$ nanocrystals showing PLQY values of 60% and 55%, respectively, after 12 months. This underscores the robust protective properties of the polymer shell surrounding the nanocrystals.

To fully assess the potential of capsules for cell labeling, a low concentration—1000 times below the toxicity threshold for Pb and Cs ions—was selected, and the cells were incubated for 24 h. The capsules demonstrated excellent biocompatibility, with no statistically significant cytotoxicity observed. The uptake of the capsules was clearly evident as their green fluorescence was detected after all incubation periods when excited at 400 nm. The sustained emission observed within the acidic lysosomal environment of the cells further confirms the suitability of these capsules for cellular and bioimaging applications. This property offers distinct advantages over conventional fluorescent dyes, especially due to the photostability of these inorganic nanocrystals in aqueous environments. Consequently, the methodology presented in this study significantly expands the potential applications of these luminescent materials, particularly in the fields of biology and biomedicine.

The previously discussed cases involve utilizing UV light to excite halide perovskite nanocrystals, resulting in visible light emission for bioimaging applications. However, in practical applications, UV light has limited penetration through the skin, which poses challenges in reaching deeper tissues [92,93]. In contrast to fluorescence-based techniques, X-Ray attenuation-based imaging offers virtually no limitations in penetration depth [94–97]. Conventional X-Ray imaging, such as chest X-Rays, presents several advantages, including lower cost, significantly reduced radiation exposure, and broader accessibility, compared to more advanced X-Ray techniques like computed tomography (CT). However, leveraging conventional X-Ray imaging as a novel modality for detecting deep-seated cancers requires the development of highly X-Ray-attenuating, cancer-specific nanomaterials [98,99].

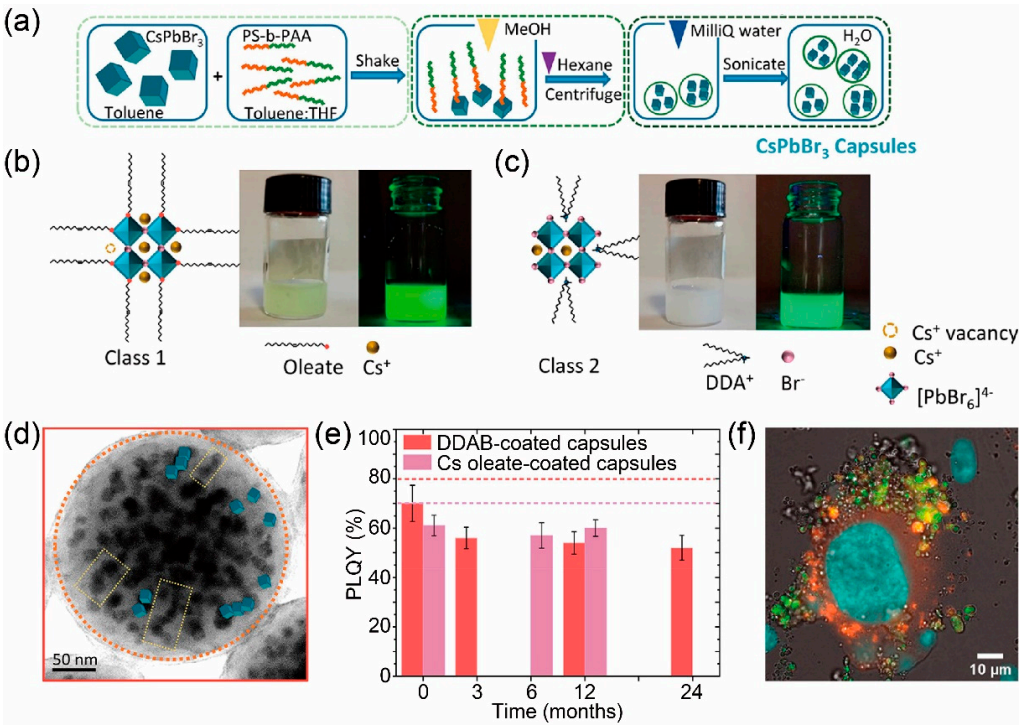

Figure 6. (**a**) A schematic illustration outlines the room-temperature fabrication process for polymer capsules containing $CsPbBr_3$ nanocrystals. This procedure involves encapsulating the nanocrystals within a water-soluble polymer matrix, ensuring both protection and enhanced stability. The photographs in (**b**,**c**) showcase aged samples of Cs–oleate-coated and didodecyl dimethylammonium bromide (DDAB)-coated $CsPbBr_3$ nanocrystals, respectively, encapsulated in polymer capsules and dispersed in deionized water. Images taken under both daylight and UV light demonstrate that both samples retain strong photoluminescence, highlighting their superior emission stability even after prolonged incubation in water. (**d**) A magnified TEM image provides a detailed view of a single polymer capsule. The embedded sketches illustrate the random distribution of $CsPbBr_3$ nanocrystals within the capsule matrix, as well as the presence of aggregated structures. These aggregates, identified as nanocrystal clusters, are highlighted with yellow frames, emphasizing their spatial arrangement within the polymer shell. (**e**) The graph plots the PLQY of polymer-encapsulated $CsPbBr_3$ nanocrystals dispersed in water over several months. Dotted lines represent the PLQY of un-encapsulated nanocrystals in toluene prior to encapsulation. (**f**) Confocal fluorescence images show cells incubated for 24 h in a medium containing $CsPbBr_3$ nanocrystals encapsulated with Cs–oleate coating. The images were captured using an excitation wavelength of 400 nm. Cell nuclei were stained with DAPI dye, which emits a blue fluorescence signal, providing a clear contrast against the bright green fluorescence emitted by the encapsulated nanocrystals. Reprinted with permission from ref. [91]. Copyright 2022, American Chemical Society.

In a recent investigation, $CsPbBr_3$ perovskite nanocrystals were selected due to their proven ability to attenuate X-Rays, positioning them as effective scintillators in conventional X-Ray detection panels [100]. The nanocrystals are rapidly co-synthesized and double-encapsulated within SiO_2, forming $CsPbBr_3$–SiO_2@SiO_2 nanoparticles that efficiently prevent aggregation, degradation, or leakage. These nanoparticles are subsequently conjugated with antibodies (Ab), yielding $CsPbBr_3$–SiO_2@SiO_2–Ab nanoparticles, which are specifically designed to target pancreatic cancer cells. The underlying methodology for attenuation-based in vivo cancer imaging via X-Ray inspection is illustrated in Figure 7a. Upon introduction of the antibody-conjugated nanoparticles into xenograft mice, the X-Ray scintillating nanocrystals within the particles significantly attenuate the incident X-Ray photons, resulting in pronounced contrast at the cancerous site (Figure 7b). An innovative and streamlined synthetic route for encapsulating $CsPbBr_3$ nanocrystals within SiO_2

nanoparticles has been developed. This process involves the rapid injection of a nanocrystal precursor solution, containing a base catalyst for SiO_2 synthesis, into a silicon precursor solution. This triggers the base-catalyzed formation of SiO_2 nanoparticles while simultaneously facilitating the ligand-assisted re-precipitation of $CsPbBr_3$ nanocrystals within a remarkably short time frame. The resulting $CsPbBr_3$–SiO_2 nanoparticles exhibit a spherical morphology, with diameters ranging from 20 to 30 nm, as confirmed by TEM images (Figure 7c–e).

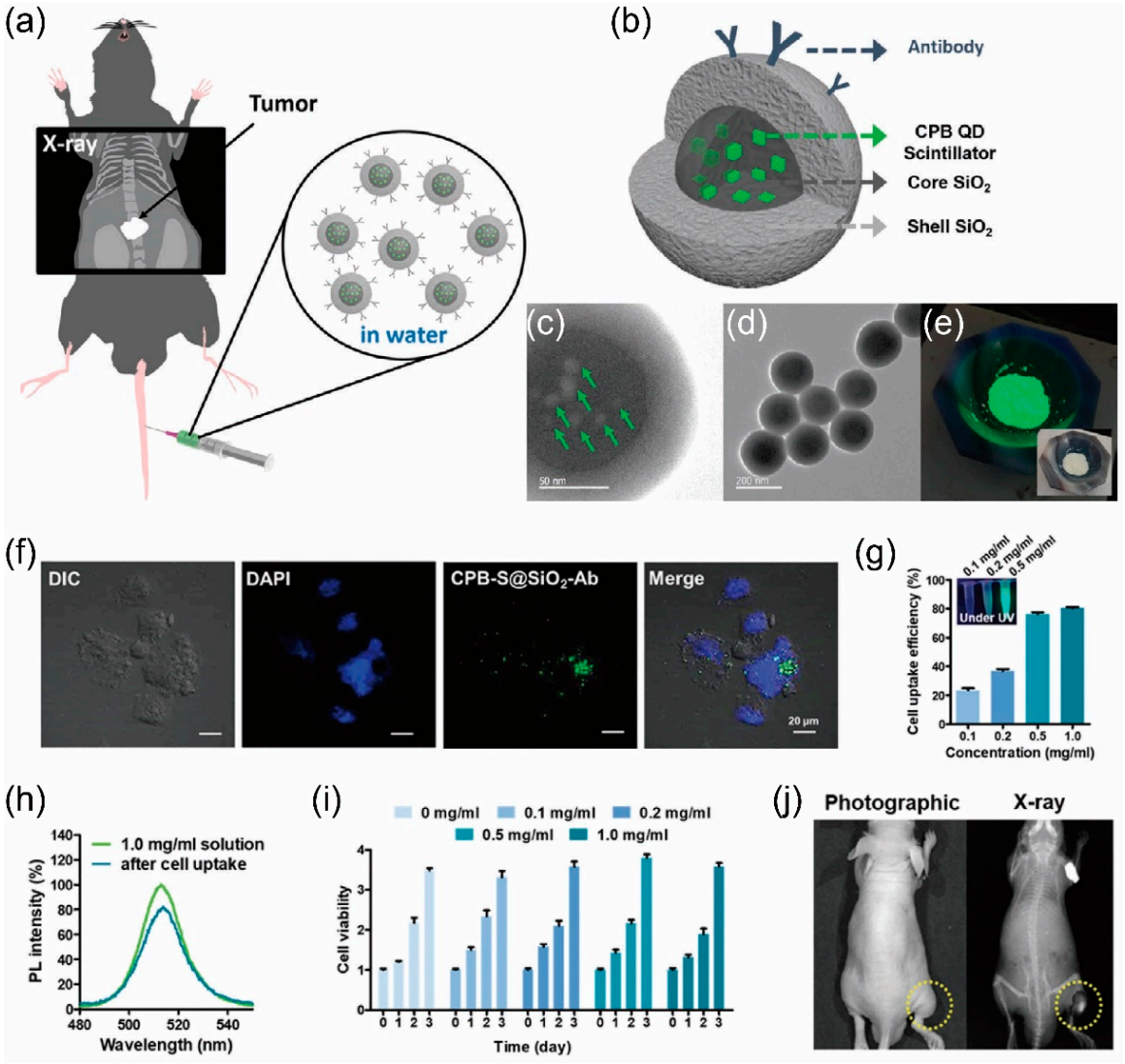

Figure 7. Schematic representation of (**a**) the cancer detection process and (**b**) the structure of $CsPbBr_3$–SiO_2@SiO_2–Ab nanoparticles. TEM images of $CsPbBr_3$–SiO_2@SiO_2 nanoparticles captured at (**c**) high and (**d**) low magnifications. (**e**) Photographs of $CsPbBr_3$–SiO_2@SiO_2 nanoparticle powder under UV light and ambient daylight. (**f**) Confocal laser scanning microscopy images of Panc-1 cells treated with $CsPbBr_3$–SiO_2@SiO_2–Ab nanoparticles. Cell nuclei are stained with blue DAPI, while the nanoparticles are visualized in green. (**g**) Cellular uptake efficiencies assessed via photoluminescence of Panc-1 cells treated with varying concentrations of nanoparticles. (**h**) Photoluminescence spectra of nanoparticle solutions and Panc-1 cells treated with the same solution. (**i**) Cell viability, as determined by the WST-1 assay, following treatment with different concentrations of nanoparticle solutions. (**j**) In vivo photographic and X-Ray images of pancreatic tumor-bearing mice taken 2 h after intravenous injection of $CsPbBr_3$–SiO_2@SiO_2–Ab nanoparticles. Reprinted with permission from ref. [100]. Copyright 2021, Wiley-VCH GmbH.

To target the CD44 surface adhesion receptor on pancreatic cells, the surfaces of the synthesized $CsPbBr_3$–SiO_2@SiO_2 nanoparticles were functionalized with anti-CD44 antibodies. Given that Cluster of Differentiation 44 (CD44) expression is often linked to poor prognosis, it serves as a critical prognostic marker and therapeutic target for pancreatic cancer. The uptake of $CsPbBr_3$–SiO_2@SiO_2–Ab nanoparticles in Panc-1 cells was assessed using confocal laser-scanning microscopy (Figure 7f). The nuclei of the cells were stained with DAPI, which emits in the blue spectral range. The PL intensities of the Panc-1 cells, reflecting the uptake of $CsPbBr_3$ nanocrystals, steadily increased as the concentration of nanoparticles rose but plateaued thereafter with no further significant increase (Figure 7g). For the 1 mg mL^{-1} solution, the maximum uptake reached 76.8% (Figure 7h). Figure 7i depicts the effect of SiO_2@SiO_2–Ab nanoparticles on the viability of Panc-1 cells, as determined by the water-soluble tetrazolium salt assay. No cytotoxicity was observed under the cell culture conditions, nor was there any noticeable effect on cell proliferation or differentiation. The non-toxicity of the $CsPbBr_3$–SiO_2@SiO_2–Ab nanoparticles clearly indicates that minimal Pb was released from the nanoparticles.

Once the transplanted Panc-1 cells had reached a sufficient size in the xenograft mouse model, a solution of $CsPbBr_3$–SiO_2@SiO_2–Ab nanoparticles was intravenously administered. As shown in Figure 7j, distinct white signals were observed at the tumor site under X-Ray irradiation, indicating that the antibody-conjugated nanoparticles successfully targeted the CD44 prognostic markers. More importantly, this result demonstrates the feasibility of detecting cancer in vivo using straightforward plain X-Ray imaging. Additionally, the real-time biodistribution of the injected $CsPbBr_3$–SiO_2@SiO_2–Ab nanoparticles was monitored via X-Ray imaging. The signal intensity increased steadily over time, peaking 2 h post-injection, and subsequently declined gradually. These findings suggest that the approach outlined in this study holds significant potential for real-time in vivo cancer detection. Note that implanting pancreatic tumors in the mouse leg (Figure 7j) is primarily for the convenience of experimental procedures and the reliability of data. Although this differs from the tumor's natural growth environment, it remains a widely used experimental method [101–104].

While halide perovskite nanocrystals show promise for deep-tissue in vivo bioimaging under X-Ray excitation, radiation exposure remains an inescapable challenge in practical applications [105–108]. As a result, researchers are increasingly exploring alternative, non-damaging excitation sources that can enable the use of halide perovskites for bioimaging without causing harm to tissues. NIR laser technology, which can be precisely focused within a localized region, offers numerous advantages, including high spatial resolution, substantial tissue penetration depth, minimal background fluorescence, and reduced photodamage to biological tissues [109–111]. Recent advances in fluorescence imaging using NIR light—particularly in the second near-infrared window (NIR-II, 900–1700 nm)—have spurred significant progress, owing to its superior tissue penetration (1–10 cm) and enhanced spatial resolution compared to visible or UV light (0.1–2 mm) [112–114]. This is primarily due to its reduced tissue absorption, scattering, and auto-fluorescence. Nevertheless, fluorescence-based imaging techniques still face considerable challenges, including the limited penetration depth of both absorption and emission light, as well as the trade-off between imaging depth and resolution.

Two-photon fluorescence imaging, which utilizes the simultaneous absorption of two NIR photons as the excitation source to generate visible light emission, is considered a highly effective technique for monitoring cellular dynamics and detecting early pathological changes [115,116]. In recent years, biological imaging under NIR illumination using lanthanide-doped nanoparticles, aggregation-induced emission nanoparticles, and II-VI quantum dots has attracted considerable attention [117–119]. In the field of halide

perovskite nanocrystals, this bioimaging approach has also been demonstrated [120–122]. In a recent study, individual $CsPbBr_3$ perovskite nanocrystals were encapsulated within silica nanoshells to effectively prevent the leakage of Pb^{2+} ions (Figure 8a) [123]. TEM images confirmed the successful coating of SiO_2 protective shells on the $CsPbBr_3$ nanocrystals (Figure 8b). The two-photon and one-photon photoluminescence properties of these nanocrystals, along with their potential applications in bioimaging, were comprehensively investigated through optical characterization and two-photon cellular imaging experiments. Figure 8c illustrates the fundamental mechanisms of light absorption and photoluminescence. In the two-photon process, a single NIR photon (800 nm) with an energy of 1.55 eV is insufficient for a direct inter-band transition, given that the calculated bandgap of $CsPbBr_3$ is 2.34 eV. Consequently, two photons are required to excite an electron from the valence band (VB) to the conduction band (CB). Following relaxation within the bands, the electrons and holes reach their respective band edges, resembling the process in single-photon excitation above the bandgap, resulting in green photoluminescence with a peak at 526 nm. Simultaneously, some electrons and holes recombine non-radiatively.

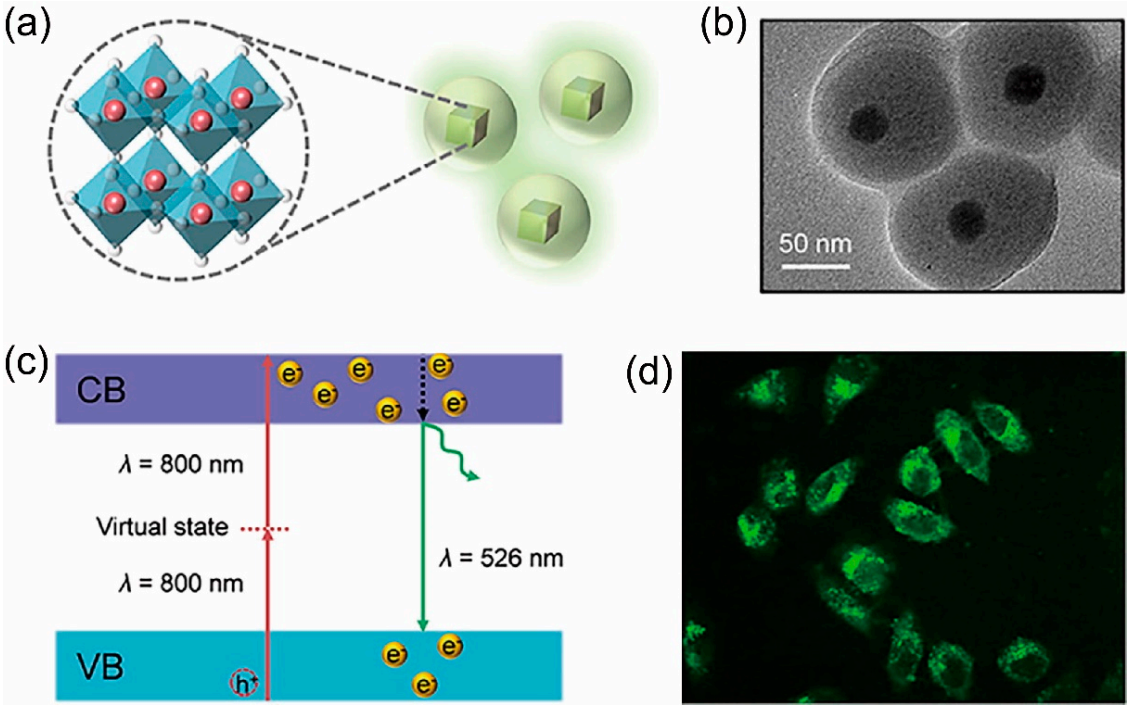

Figure 8. (**a**) Schematic illustration of $CsPbBr_3$@SiO_2 core–shell nanocrystals engineered for two-photon bioimaging applications. (**b**) TEM images of the as-prepared $CsPbBr_3$@SiO_2 nanocrystals. (**c**) Schematic representation depicting the two-photon absorption and subsequent emission process in $CsPbBr_3$@SiO_2 nanocrystals. (**d**) Fluorescence image of HepG2 cells from the experimental group under 800 nm NIR illumination, demonstrating enhanced luminescent activity. Reprinted with permission from ref. [123]. Copyright 2022, Elsevier.

To evaluate the potential application of $CsPbBr_3$@SiO_2 nanocrystals in two-photon fluorescence biological imaging, HepG2 cells were incubated with $CsPbBr_3$@SiO_2 for 24 h. Under 800-nm laser scanning, the control group of HepG2 cells exhibited minimal fluorescence, while the experimental group emitted bright green fluorescence due to two-photon absorption (Figure 8d). This suggests that the cellular luminescence signals originated from $CsPbBr_3$@SiO_2 nanocrystals that were internalized into the cells via endocytosis. These findings highlight that $CsPbBr_3$@SiO_2 nanocrystals, as two-photon imaging nanoprobes,

could effectively minimize interference from cellular auto-fluorescence, ensuring high-quality imaging.

Other studies have also explored the use of halide perovskite nanocrystals for two-photon up-conversion bioimaging. For instance, it has been demonstrated that antibody-functionalized 1D $CsPbBr_3$ nanowires, 2D $CsPbBr_3$ nanoplatelets, and 3D $CsPbBr_3$ nanocubes can be employed for selective and simultaneous two-photon imaging of heterogeneous breast cancer cells within the NIR biological window [124–126]. These biocompatible nanostructures can be fabricated by coating them with amine-functionalized poly(ethylene glycol)-propionic acid. Remarkably, over 86% of the photoluminescence intensity is retained by these nanocrystals after 35 days submerged in water, showcasing exceptional photostability by maintaining 99% of the photoluminescence intensity after 3 h of UV light exposure. Furthermore, antibody-conjugated 1D and 2D perovskite nanomaterials have demonstrated the ability to perform simultaneous two-photon imaging of triple-negative breast cancer cells and human epidermal growth factor receptor 2 (HER2)-positive breast cancer cells.

3. Halide Perovskite Nanocrystals for Chemical Sensing Applications

Halide perovskite nanocrystals have not only led to pioneering advancements in the field of bioimaging but have also achieved notable outcomes in chemical sensing, particularly in the analysis and detection of metabolic products [127–129]. As illustrated in Figure 9, a recent study reports the synthesis of $CsPbCl_3$:Mn^{2+}@SiO_2 core–shell nanoparticles in water solutions, which was accomplished through the usage of capping ligand, surface modification, and crystal engineering strategies [130]. The SN_2 reaction between 4-chlorobutyric acid (CBA) and oleylamine (OAm) generates a zwitterionic ligand that promotes the dispersion of $CsPbCl_3$:Mn^{2+}@SiO_2 nanoparticles, while the robust SiO_2 shell significantly improves their overall stability. Furthermore, Mn^{2+} doping introduces a secondary emission center while enabling potential postsynthetic modifications. This transformation results in the formation of MnO_2@$CsPbCl_3$:Mn^{2+}@SiO_2 nanoparticles, which exhibit remarkable oxidase (OXD)-like activity. Theoretical calculations suggest that electron transfer from $CsPbCl_3$ to in situ MnO_2, combined with the adsorption–desorption process of 3,3′,5,5′-tetramethylbenzidine (TMB), significantly enhances the OXD-like activity. Mn^{4+} in MnO_2@$CsPbCl_3$:Mn^{2+}@SiO_2 (fluorescent nanozyme) is reduced to Mn^{2+} and dissociates in the presence of ascorbic acid (AA), thus inhibiting OXD-like activity and triggering fluorescence "turn-on/off" behavior, enabling dual-mode recognition. Ultimately, a biomarker detection platform based on the MnO_2@$CsPbCl_3$:Mn^{2+}@SiO_2 fluorescent nanozyme is established, with AA serving as the reporter molecule, enabling the precise detection of human serum alkaline phosphatase (ALP). This demonstrates the considerable potential of perovskites in biosensing applications.

The sensitive detection of *Staphylococcus aureus* enterotoxins (SEs) is essential for food inspection because of their high pathogenicity, which can be achieved through surface-enhanced Raman scattering (SERS) utilizing SERS-active nanostructures [126,131,132]. As illustrated in Figure 10, a recent study developed an Au–Ag Janus nanoparticle/$CsPbBr_3$ composite-based SERS immunoassay for SE detection [133]. The plasmonic Au–Ag Janus nanoparticles exhibited inherent SERS activity facilitated by 2-mercaptobenzoimidazole-5-carboxylic acid ligands. $CsPbBr_3$@mesoporous silica nanomaterials (MSNs) were synthesized and subsequently converted into $CsPb_2Br_5$@MSNs in the aqueous phase. Paired SE antibody–antigen-driven plasmonic Au–Ag Janus nanoparticle–$CsPb_2Br_5$@MSN composites were then prepared. These composites displayed enhanced SERS activity, which was attributed to the suppression of plasmonic decay through electromagnetic field enhancement and electron transfer mechanisms. A positive correlation was established between the

SERS signals and SE concentrations of the composites. An additive-free SERS immunoassay was developed for the straightforward, sensitive, and reproducible detection of SEs. This study lays the groundwork for the development of multiple additive-free SERS-active plasmonic nanoparticle/perovskite composites, opening new avenues for the exploration of SERS-based detection probes in food safety monitoring.

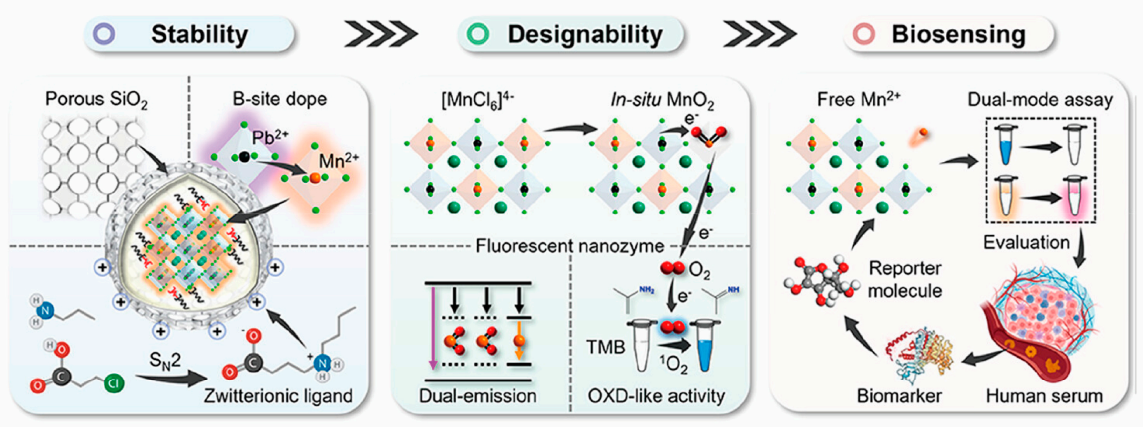

Figure 9. Schematic representation of the trinity strategy that empowers $CsPbCl_3$ nanocrystals to function as hydrophilic and highly efficient fluorescent nanozymes for the development of biomarker reporting platforms. Reprinted with permission from ref. [130]. Copyright 2024, American Chemical Society.

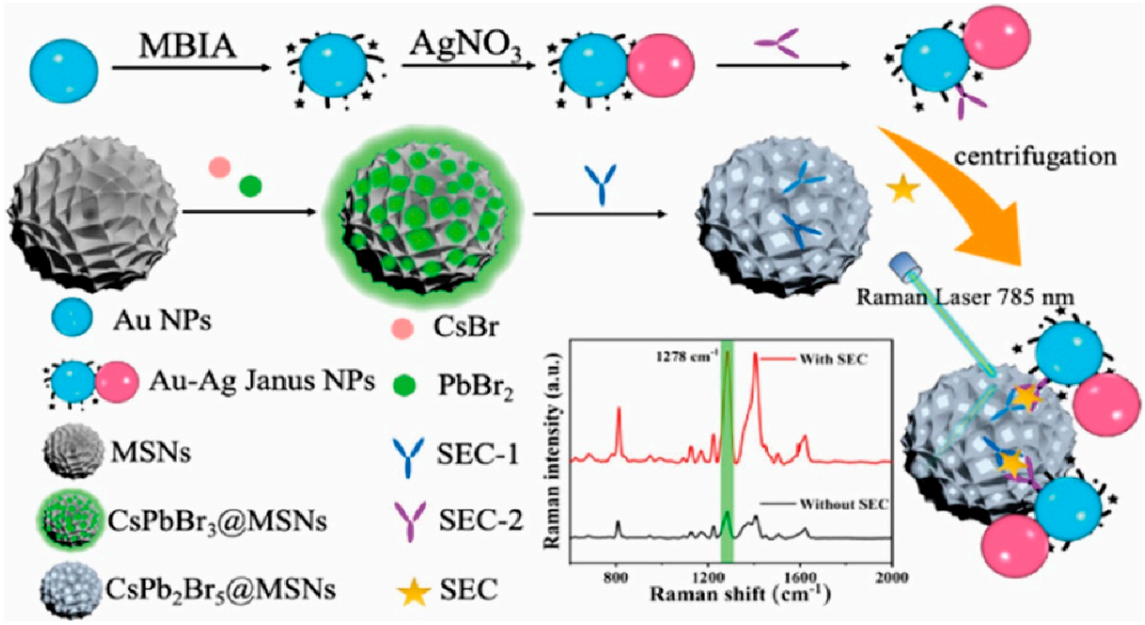

Figure 10. Schematic representation of SERS-active composites featuring Au–Ag Janus nanoparticles/$CsPbBr_3$ for immunoassays targeting Staphylococcus aureus enterotoxins. Reprinted with permission from ref. [133]. Copyright 2022, American Chemical Society.

Dual-functional perovskite nanomaterials with both hydrogen sulfide (H_2S)-sensing and antibacterial properties hold significant promise. As shown in Figure 11, chiral halide perovskite nanomaterials (R/S-α-PEA)$_2CsPb_2Br_7$ were synthesized and evenly dispersed in aqueous solution [134]. The encapsulation of methoxypolyethylene glycol amine (mPEG-NH_2) enhanced the water stability and uniformity of the particle size. The incorporation of chiral cations successfully induced circular dichroism (CD) signals. As probes, these perovskites demonstrated a rapid and sensitive luminescence quenching response to H_2S,

with imaging detection being performed at the *Escherichia coli* (*E. coli*) level. Moreover, their strong positive charge properties as antibacterial agents promotes membrane lysis, resulting in E. coli cell death and showcasing significant antibacterial effects. This work represents a preliminary exploration into the use of chiral perovskites in biological applications, providing valuable insights into the development of bi-functional perovskite nanomaterials for biological sensing and antibacterial treatments.

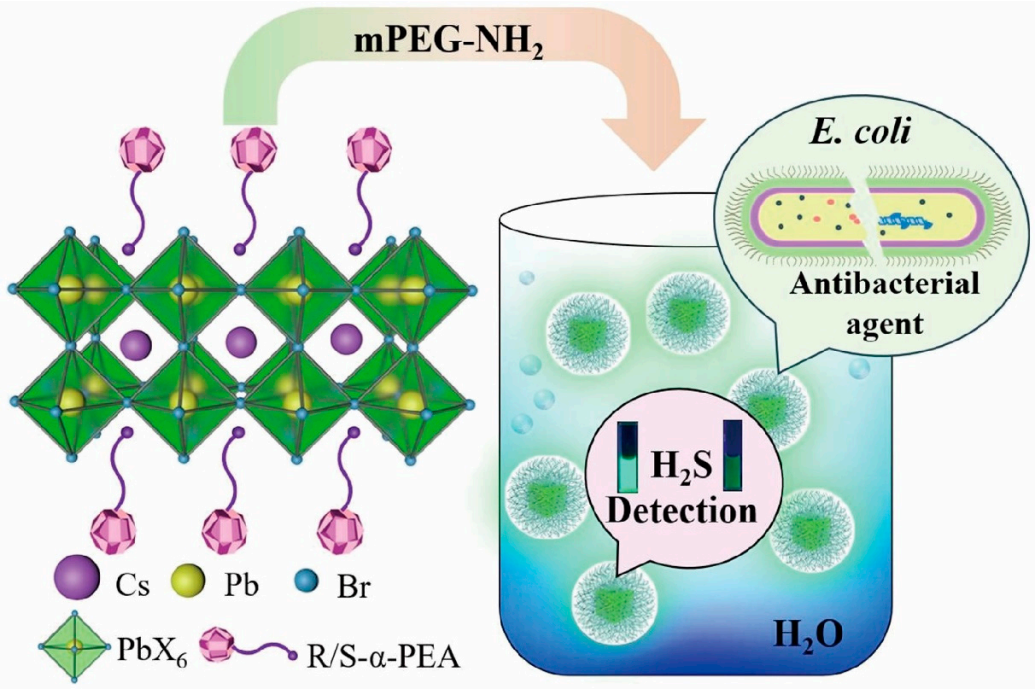

Figure 11. Liquid-phase dual-functional chiral perovskites have been developed for both hydrogen sulfide (H_2S) detection and antibacterial applications against *Escherichia coli*. Reprinted with permission from ref. [134]. Copyright 2024, Elsevier.

Similarly, $CsPbBr_3$ nanocrystals have been innovatively encapsulated within nanomicelles formed from a polyethylene glycol–polycaprolactone (PEG-PCL) block copolymer, resulting in biocompatible $CsPbBr_3$ nanocrystals with exceptional water resistance [135]. Thanks to their superior water resistance and biocompatibility, these $CsPbBr_3$ nanocrystals are ideal for real-time, long-term quantitative monitoring of H_2S levels in living cell and zebrafish models.

In another study, phospholipid membrane (PM)-coated $CsPbX_3$ nanocrystals exhibiting intrinsic bio-catalytic activity were discovered [136]. Unlike other peroxidase-like nanozymes that rely on external chromogenic reagents, the PM-$CsPbX_3$ nanocrystals function as self-reporting nanoprobes, enabling an "add-to-answer" detection model. Remarkably, the fluorescence of PM-$CsPbX_3$ nanocrystals is rapidly quenched upon the addition of H_2O_2 and can be restored by removing excess H_2O_2 (Figure 12a). This unexpected observation opens new possibilities for using PM-$CsPbX_3$ nanocrystals in the development of multicolor bio-inks and metabolite-responsive paper analytical devices, showcasing their significant potential in bioanalysis (Figure 12b). This is the first report of the nanozyme-like properties of $CsPbX_3$ perovskite nanocrystals, marking a major advancement in the nanozyme field and paving the way for novel in vitro disease diagnostic applications.

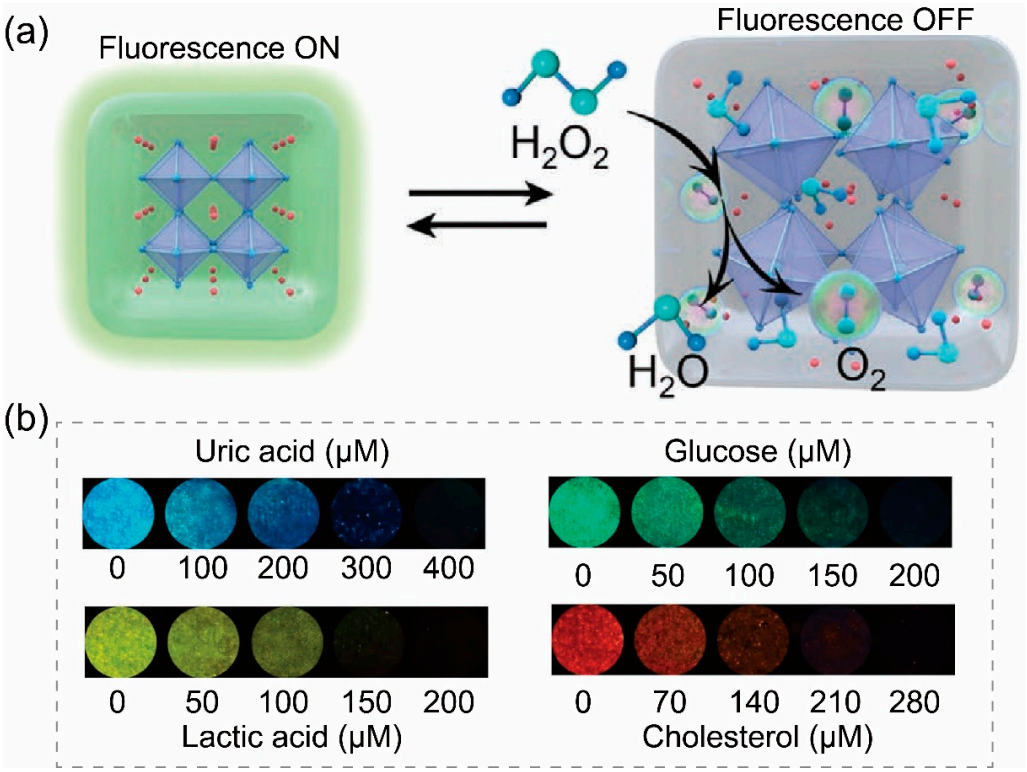

Figure 12. (**a**) Schematic of the bio-catalytic activity of PM-$CsPbX_3$ nanocrystals. (**b**) Photographs of oxidase/PM-$CsPbX_3$ nanocrystals materials with different substrates under UV light. Reprinted with permission from ref. [136]. Copyright 2021, Wiley-VCH GmbH.

4. Halide Perovskite Nanocrystals for Other Novel Applications

Quantitative fluorescence immunoassays are vital for point-of-care testing in food safety and clinical healthcare [137]. However, existing labeling materials, ranging from organic luciferins to quantum dots, often fall short in meeting the increasing demand for multi-target detection due to their broad emission spectra [138,139]. In a recent study, researchers introduced halide perovskite nanocrystals as novel labeling materials, which feature a narrower photoluminescence spectrum [140]. A sensitive and quantitative immunoassay method, the perovskite nanocrystal fluorescence-linked immunosorbent assay, was also demonstrated. To achieve stable and water-dispersible halide perovskite nanocrystals, they were functionalized with hydroxyl groups. Perovskite antibodies as fluorescent probes were created through electrostatic adsorption with a narrow FWHM of 18 nm, laying the groundwork for future multi-target detection applications. Both indirect competitive and sandwich immunoassays were successfully demonstrated. This work presents a promising labeling material for point-of-care tests and paves the way for the next generation of immunoassays.

Single-molecule localization microscopy is crucial for visualizing cellular microstructures [141,142]. However, existing microscopy imaging materials, such as organic fluorophores and quantum dots, often fail to meet the increasing demand for multi-target detection due to their broad emission spectra [143]. In a recent study, a core–shell nanocomposite, $CsPb(ClBr)_3$@PEG, was introduced [144]. This probe was synthesized through a one-step encapsulation of hydrophilic $CsPbBr_3$ nanocrystals into functionalized PEG. The resulting material exhibits wavelength tunability with a narrow FWHM of 11 nm. The PEG shell provides broad spectral tunability, superior photostability lasting several years, and the potential for further surface functionalization. $CsPb(ClBr)_3$@PEG achieves high localization precision and a tenfold improvement in spatial resolution. When applied to imaging

exosomes, this probe successfully distinguished two adjacent exosomes. Furthermore, after biotin modification, $CsPb(ClBr)_3$@PEG proved versatile for microscopy imaging of cellular microstructures. Its remarkable photostability and narrow FWHM suggest that this $CsPbBr_3$-based nanoprobe holds significant potential as a commercial dye for multi-target super-resolution bioimaging.

5. Conclusions and Perspectives

Halide perovskite nanocrystals have garnered considerable attention in the biomedical field due to their excellent optical properties, including high quantum yields, tunable emission wavelengths, and narrow emission spectra. These characteristics make them ideal candidates for applications such as bioimaging and chemical sensing. However, despite their promising potential, several significant challenges remain, particularly concerning their metabolic pathways, which limit their widespread use in biomedical applications. Notably, the metabolic behavior of halide perovskite nanocrystals within the body, their eventual degradation products, and their potential systemic toxicity are not yet well understood. Addressing these issues will be essential for ensuring the safe and effective use of these materials in clinical settings. Below are some of the challenges and future research directions regarding the use of halide perovskite nanocrystals in biomedical applications.

Unclear Metabolic Pathways and Degradation Products: One of the most critical concerns when using nanomaterials in biomedical applications is understanding how these materials are metabolized by the body. In the case of halide perovskite nanocrystals, there is currently a lack of clarity regarding their metabolic pathways in vivo [145]. It remains unclear how these nanocrystals are processed by the body, where they accumulate, and how they are ultimately excreted. This uncertainty complicates the prediction of long-term effects and the optimization of perovskite-based materials for in vivo use. Therefore, future research should focus on understanding the metabolic pathways of halide perovskite nanocrystals in vivo. Studies that track the distribution, metabolism, and excretion of these nanocrystals will be essential for assessing their safety and efficacy. Advanced imaging techniques, such as in vivo fluorescence tracking and mass spectrometry, could be employed to monitor the fate of perovskite nanocrystals in living organisms. Additionally, identifying the degradation products of perovskite nanocrystals and assessing their toxicity will be critical.

Bioaccumulation and Clearance: Another major issue is the potential for the bioaccumulation of halide perovskite nanocrystals in the body. If the nanocrystals are not efficiently cleared by the body after use, they could accumulate in various organs, leading to chronic toxicity. The bioaccumulation of nanomaterials depends on factors such as particle size, surface charge, and surface functionalization. However, these factors are not well understood in the context of halide perovskite nanocrystals. Moreover, research on the clearance mechanisms of these nanocrystals is still in its infancy, and the routes by which these materials are eliminated from the body remain unclear. Therefore, extensive studies are needed to understand how halide perovskite nanocrystals are cleared from the body. Investigating the bioaccumulation potential of these nanocrystals in various organs, as well as their clearance pathways, will provide crucial information on their long-term safety. Nanomaterials that are easily cleared from the body are less likely to pose risks, so research into enhancing the excretion of perovskite nanocrystals (through renal or hepatic pathways) should be prioritized. Additionally, the optimization of particle size, surface charge, and functionalization for efficient renal or lymphatic clearance could significantly reduce the risk of bioaccumulation.

Funding: This research was funded by Shandong Provincial Natural Science Foundation, grant number ZR2024QE319.

Data Availability Statement: No new data were created or analyzed in this study.

Conflicts of Interest: The authors declare no conflicts of interest.

References

1. Protesescu, L.; Yakunin, S.; Bodnarchuk, M.I.; Krieg, F.; Caputo, R.; Hendon, C.H.; Yang, R.X.; Walsh, A.; Kovalenko, M.V. Nanocrystals of Cesium Lead Halide Perovskites ($CsPbX_3$, X = Cl, Br, and I): Novel Optoelectronic Materials Showing Bright Emission with Wide Color Gamut. *Nano Lett.* **2015**, *15*, 3692–3696. [CrossRef] [PubMed]
2. Nedelcu, G.; Protesescu, L.; Yakunin, S.; Bodnarchuk, M.I.; Grotevent, M.J.; Kovalenko, M.V. Fast Anion-Exchange in Highly Luminescent Nanocrystals of Cesium Lead Halide Perovskites ($CsPbX_3$, X = Cl, Br, I). *Nano Lett.* **2015**, *15*, 5635–5640. [CrossRef] [PubMed]
3. Dey, A.; Ye, J.; De, A.; Debroye, E.; Ha, S.K.; Bladt, E.; Kshirsagar, A.S.; Wang, Z.; Yin, J.; Wang, Y.; et al. State of the Art and Prospects for Halide Perovskite Nanocrystals. *ACS Nano* **2021**, *15*, 10775–10981. [CrossRef] [PubMed]
4. Zhang, F.; Zhong, H.; Chen, C.; Wu, X.; Hu, X.; Huang, H.; Han, J.; Zou, B.; Dong, Y. Brightly Luminescent and Color-Tunable Colloidal CH_3 NH_3 PbX_3 (X = Br, I, Cl) Quantum Dots: Potential Alternatives for Display Technology. *ACS Nano* **2015**, *9*, 4533–4542. [CrossRef]
5. Song, P.; Qiao, B.; Song, D.; Cao, J.; Shen, Z.; Xu, Z.; Zhao, S.; Wageh, S.; Al-Ghamdi, A. Modifying the Crystal Field of $CsPbCl_3$:Mn^{2+} Nanocrystals by Co-Doping to Enhance Its Red Emission by a Hundredfold. *ACS Appl. Mater. Interfaces* **2020**, *12*, 30711–30719. [CrossRef]
6. Hu, M.; Jia, S.; Liu, Y.; Cui, J.; Zhang, Y.; Su, H.; Cao, S.; Mo, L.; Chu, D.; Zhao, G.; et al. Large and Dense Organic–Inorganic Hybrid Perovskite CH_3 NH_3 PbI_3 Wafer Fabricated by One-Step Reactive Direct Wafer Production with High X-Ray Sensitivity. *ACS Appl. Mater. Interfaces* **2020**, *12*, 16592–16600. [CrossRef]
7. Yuan, R.; Shen, L.; Shen, C.; Liu, J.; Zhou, L.; Xiang, W.; Liang, X. $CsPbBr_3$: *X* Eu^{3+} Perovskite QD Borosilicate Glass: A New Member of the Luminescent Material Family. *Chem. Commun.* **2018**, *54*, 3395–3398. [CrossRef]
8. Raja, S.N.; Bekenstein, Y.; Koc, M.A.; Fischer, S.; Zhang, D.; Lin, L.; Ritchie, R.O.; Yang, P.; Alivisatos, A.P. Encapsulation of Perovskite Nanocrystals into Macroscale Polymer Matrices: Enhanced Stability and Polarization. *ACS Appl. Mater. Interfaces* **2016**, *8*, 35523–35533. [CrossRef]
9. Mendoza-Carreño, J.; Molet, P.; Otero-Martínez, C.; Alonso, M.I.; Polavarapu, L.; Mihi, A. Nanoimprinted 2D-Chiral Perovskite Nanocrystal Metasurfaces for Circularly Polarized Photoluminescence. *Adv. Mater.* **2023**, *35*, 2210477. [CrossRef]
10. Song, J.; Li, J.; Li, X.; Xu, L.; Dong, Y.; Zeng, H. Quantum Dot Light-Emitting Diodes Based on Inorganic Perovskite Cesium Lead Halides ($CsPbX_3$). *Adv. Mater.* **2015**, *27*, 7162–7167. [CrossRef]
11. Meinardi, F.; Akkerman, Q.A.; Bruni, F.; Park, S.; Mauri, M.; Dang, Z.; Manna, L.; Brovelli, S. Doped Halide Perovskite Nanocrystals for Reabsorption-Free Luminescent Solar Concentrators. *ACS Energy Lett.* **2017**, *2*, 2368–2377. [CrossRef] [PubMed]
12. Sun, R.; Lu, P.; Zhou, D.; Xu, W.; Ding, N.; Shao, H.; Zhang, Y.; Li, D.; Wang, N.; Zhuang, X.; et al. Samarium-Doped Metal Halide Perovskite Nanocrystals for Single-Component Electroluminescent White Light-Emitting Diodes. *ACS Energy Lett.* **2020**, *5*, 2131–2139. [CrossRef]
13. Gualdrón-Reyes, A.F.; Masi, S.; Mora-Seró, I. Progress in Halide-Perovskite Nanocrystals with near-Unity Photoluminescence Quantum Yield. *Trends Chem.* **2021**, *3*, 499–511. [CrossRef]
14. De Trizio, L.; Infante, I.; Manna, L. Surface Chemistry of Lead Halide Perovskite Colloidal Nanocrystals. *Acc. Chem. Res.* **2023**, *56*, 1815–1825. [CrossRef]
15. Pan, G.; Bai, X.; Yang, D.; Chen, X.; Jing, P.; Qu, S.; Zhang, L.; Zhou, D.; Zhu, J.; Xu, W.; et al. Doping Lanthanide into Perovskite Nanocrystals: Highly Improved and Expanded Optical Properties. *Nano Lett.* **2017**, *17*, 8005–8011. [CrossRef]
16. Hong, W.; Huang, Y.; Chang, C.; Zhang, Z.; Tsai, H.; Chang, N.; Chao, Y. Efficient Low-Temperature Solution-Processed Lead-Free Perovskite Infrared Light-Emitting Diodes. *Adv. Mater.* **2016**, *28*, 8029–8036. [CrossRef]
17. Zhu, F.-P.; Yong, Z.-J.; Liu, B.-M.; Chen, Y.-M.; Zhou, Y.; Ma, J.-P.; Sun, H.-T.; Fang, Y.-Z. Superbroad Near-Infrared Photoluminescence from Bismuth-Doped CsPbI_3 Perovskite Nanocrystals. *Opt. Express* **2017**, *25*, 33283. [CrossRef]
18. Liang, J.; Wang, C.; Zhao, P.; Lu, Z.; Ma, Y.; Xu, Z.; Wang, Y.; Zhu, H.; Hu, Y.; Zhu, G.; et al. Solution Synthesis and Phase Control of Inorganic Perovskites for High-Performance Optoelectronic Devices. *Nanoscale* **2017**, *9*, 11841–11845. [CrossRef]
19. Zhang, B.; Guo, F.; Xue, J.; Yang, L.; Zhao, Y.; Ge, M.; Cai, Q.; Liu, B.; Xie, Z.; Chen, D.; et al. Photoluminescence Study of the Photoinduced Phase Separation in Mixed-Halide Hybrid Perovskite $CH_3NH_3Pb(Br_xI_{1-x})3$ Crystals Synthesized via a Solvothermal Method. *Sci. Rep.* **2017**, *7*, 17695. [CrossRef]
20. Zhao, H.; Hu, Z.; Wei, L.; Zeng, P.; Kuang, C.; Liu, X.; Bai, S.; Gao, F.; Liu, M. Efficient and High-Luminance Perovskite Light-Emitting Diodes Based on $CsPbBr_3$ Nanocrystals Synthesized from a Dual-Purpose Organic Lead Source. *Small* **2020**, *16*, 2003939. [CrossRef]

21. Liu, Z.; Qin, X.; Chen, Q.; Jiang, T.; Chen, Q.; Liu, X. Metal–Halide Perovskite Nanocrystal Superlattice: Self-Assembly and Optical Fingerprints. *Adv. Mater.* **2023**, *35*, 2209279. [CrossRef] [PubMed]
22. Zhou, Z.-R.; Liao, Z.-H.; Wang, F. Shape-Controlled Synthesis of One-Dimensional Cesium Lead Halide Perovskite Nanocrystals: Methods and Advances. *J. Mater. Chem. C* **2023**, *11*, 3409–3427. [CrossRef]
23. Mohammed, O.F. Outstanding Challenges of Zero-Dimensional Perovskite Materials. *J. Phys. Chem. Lett.* **2019**, *10*, 5886–5888. [CrossRef]
24. Smock, S.R.; Chen, Y.; Rossini, A.J.; Brutchey, R.L. The Surface Chemistry and Structure of Colloidal Lead Halide Perovskite Nanocrystals. *Acc. Chem. Res.* **2021**, *54*, 707–718. [CrossRef]
25. Otero-Martínez, C.; García-Lojo, D.; Pastoriza-Santos, I.; Pérez-Juste, J.; Polavarapu, L. Dimensionality Control of Inorganic and Hybrid Perovskite Nanocrystals by Reaction Temperature: From No-Confinement to 3D and 1D Quantum Confinement. *Angew. Chem.* **2021**, *133*, 26881–26888. [CrossRef]
26. Liu, J.; Zheng, X.; Mohammed, O.F.; Bakr, O.M. Self-Assembly and Regrowth of Metal Halide Perovskite Nanocrystals for Optoelectronic Applications. *Acc. Chem. Res.* **2022**, *55*, 262–274. [CrossRef]
27. Mondal, N.; De, A.; Das, S.; Paul, S.; Samanta, A. Ultrafast Carrier Dynamics of Metal Halide Perovskite Nanocrystals and Perovskite-Composites. *Nanoscale* **2019**, *11*, 9796–9818. [CrossRef]
28. Yang, B.; Han, K. Charge-Carrier Dynamics of Lead-Free Halide Perovskite Nanocrystals. *Acc. Chem. Res.* **2019**, *52*, 3188–3198. [CrossRef]
29. Kamat, P.V.; Kuno, M. Halide Ion Migration in Perovskite Nanocrystals and Nanostructures. *Acc. Chem. Res.* **2021**, *54*, 520–531. [CrossRef]
30. Ramasamy, P.; Lim, D.-H.; Kim, B.; Lee, S.-H.; Lee, M.-S.; Lee, J.-S. All-Inorganic Cesium Lead Halide Perovskite Nanocrystals for Photodetector Applications. *Chem. Commun.* **2016**, *52*, 2067–2070. [CrossRef]
31. Yan, F.; Tan, S.T.; Li, X.; Demir, H.V. Light Generation in Lead Halide Perovskite Nanocrystals: LEDs, Color Converters, Lasers, and Other Applications. *Small* **2019**, *15*, 1902079. [CrossRef] [PubMed]
32. Liu, C.; Zeng, Q.; Wei, H.; Yu, Y.; Zhao, Y.; Feng, T.; Yang, B. Metal Halide Perovskite Nanocrystal Solar Cells: Progress and Challenges. *Small Methods* **2020**, *4*, 2000419. [CrossRef]
33. Kim, Y.-H.; Wolf, C.; Kim, Y.-T.; Cho, H.; Kwon, W.; Do, S.; Sadhanala, A.; Park, C.G.; Rhee, S.-W.; Im, S.H.; et al. Highly Efficient Light-Emitting Diodes of Colloidal Metal–Halide Perovskite Nanocrystals beyond Quantum Size. *ACS Nano* **2017**, *11*, 6586–6593. [CrossRef] [PubMed]
34. Akkerman, Q.A.; Rainò, G.; Kovalenko, M.V.; Manna, L. Genesis, Challenges and Opportunities for Colloidal Lead Halide Perovskite Nanocrystals. *Nat. Mater.* **2018**, *17*, 394–405. [CrossRef]
35. Ochsenbein, S.T.; Krieg, F.; Shynkarenko, Y.; Rainò, G.; Kovalenko, M.V. Engineering Color-Stable Blue Light-Emitting Diodes with Lead Halide Perovskite Nanocrystals. *ACS Appl. Mater. Interfaces* **2019**, *11*, 21655–21660. [CrossRef]
36. Liu, D.; Guo, Y.; Que, M.; Yin, X.; Liu, J.; Xie, H.; Zhang, C.; Que, W. Metal Halide Perovskite Nanocrystals: Application in High-Performance Photodetectors. *Mater. Adv.* **2021**, *2*, 856–879. [CrossRef]
37. Surendran, A.; Yu, X.; Begum, R.; Tao, Y.; Wang, Q.J.; Leong, W.L. All Inorganic Mixed Halide Perovskite Nanocrystal–Graphene Hybrid Photodetector: From Ultrahigh Gain to Photostability. *ACS Appl. Mater. Interfaces* **2019**, *11*, 27064–27072. [CrossRef]
38. Zhang, Q.; Yin, Y. All-Inorganic Metal Halide Perovskite Nanocrystals: Opportunities and Challenges. *ACS Cent. Sci.* **2018**, *4*, 668–679. [CrossRef]
39. Zhong, F.; He, Y.; Sun, Y.; Dong, F.; Sheng, J. Metal-Doping of Halide Perovskite Nanocrystals for Energy and Environmental Photocatalysis: Challenges and Prospects. *J. Mater. Chem. A* **2022**, *10*, 22915–22928. [CrossRef]
40. Shyamal, S.; Pradhan, N. Halide Perovskite Nanocrystal Photocatalysts for CO_2 Reduction: Successes and Challenges. *J. Phys. Chem. Lett.* **2020**, *11*, 6921–6934. [CrossRef]
41. Zhou, L.; Xu, Y.; Chen, B.; Kuang, D.; Su, C. Synthesis and Photocatalytic Application of Stable Lead-Free Cs_2 $AgBiBr_6$ Perovskite Nanocrystals. *Small* **2018**, *14*, 1703762. [CrossRef] [PubMed]
42. Wang, J.; Shi, Y.; Wang, Y.; Li, Z. Rational Design of Metal Halide Perovskite Nanocrystals for Photocatalytic CO_2 Reduction: Recent Advances, Challenges, and Prospects. *ACS Energy Lett.* **2022**, *7*, 2043–2059. [CrossRef]
43. Cortés-Villena, A.; Bellezza, D.; Cunha, C.; Rosa-Pardo, I.; Seijas-Da Silva, Á.; Pina, J.; Abellán, G.; Seixas De Melo, J.S.; Galian, R.E.; Pérez-Prieto, J. Engineering Metal Halide Perovskite Nanocrystals with BODIPY Dyes for Photosensitization and Photocatalytic Applications. *J. Am. Chem. Soc.* **2024**, *146*, 14479–14492. [CrossRef] [PubMed]
44. Zhang, L.; Miao, J.; Li, J.; Li, Q. Halide Perovskite Materials for Energy Storage Applications. *Adv. Funct. Mater.* **2020**, *30*, 2003653. [CrossRef]
45. Kostopoulou, A.; Brintakis, K.; Nasikas, N.K.; Stratakis, E. Perovskite Nanocrystals for Energy Conversion and Storage. *Nanophotonics* **2019**, *8*, 1607–1640. [CrossRef]
46. Narayanan, S.; Parikh, N.; Tavakoli, M.M.; Pandey, M.; Kumar, M.; Kalam, A.; Trivedi, S.; Prochowicz, D.; Yadav, P. Metal Halide Perovskites for Energy Storage Applications. *Eur. J. Inorg. Chem.* **2021**, *2021*, 1201–1212. [CrossRef]

47. Ngo, L.T.; Huang, W.; Chan, M.; Su, T.; Li, C.; Hsiao, M.; Liu, R. Comprehensive Neurotoxicity of Lead Halide Perovskite Nanocrystals in Nematode *Caenorhabditis elegans*. *Small* **2024**, *20*, 2306020. [CrossRef]
48. Infante, I.; Manna, L. Are There Good Alternatives to Lead Halide Perovskite Nanocrystals? *Nano Lett.* **2021**, *21*, 6–9. [CrossRef]
49. Babayigit, A.; Ethirajan, A.; Muller, M.; Conings, B. Toxicity of Organometal Halide Perovskite Solar Cells. *Nat. Mater.* **2016**, *15*, 247–251. [CrossRef]
50. Ren, M.; Qian, X.; Chen, Y.; Wang, T.; Zhao, Y. Potential Lead Toxicity and Leakage Issues on Lead Halide Perovskite Photovoltaics. *J. Hazard. Mater.* **2022**, *426*, 127848. [CrossRef]
51. Patsiou, D.; Del Rio-Cubilledo, C.; Catarino, A.I.; Summers, S.; Mohd Fahmi, A.; Boyle, D.; Fernandes, T.F.; Henry, T.B. Exposure to Pb-Halide Perovskite Nanoparticles Can Deliver Bioavailable Pb but Does Not Alter Endogenous Gut Microbiota in Zebrafish. *Sci. Total Environ.* **2020**, *715*, 136941. [CrossRef] [PubMed]
52. Dong, Y.; Zhao, Y.; Zhang, S.; Dai, Y.; Liu, L.; Li, Y.; Chen, Q. Recent Advances toward Practical Use of Halide Perovskite Nanocrystals. *J. Mater. Chem. A* **2018**, *6*, 21729–21746. [CrossRef]
53. Zhang, J.; Zhu, Y. Exploiting the Photo-Physical Properties of Metal Halide Perovskite Nanocrystals for Bioimaging. *ChemBioChem* **2024**, *25*, e202300683. [CrossRef]
54. Yang, D.; Li, X.; Zeng, H. Surface Chemistry of All Inorganic Halide Perovskite Nanocrystals: Passivation Mechanism and Stability. *Adv. Mater. Interfaces* **2018**, *5*, 1701662. [CrossRef]
55. Li, J.; Cao, H.-L.; Jiao, W.-B.; Wang, Q.; Wei, M.; Cantone, I.; Lü, J.; Abate, A. Biological Impact of Lead from Halide Perovskites Reveals the Risk of Introducing a Safe Threshold. *Nat. Commun.* **2020**, *11*, 310. [CrossRef]
56. Liu, M.; Matuhina, A.; Zhang, H.; Vivo, P. Advances in the Stability of Halide Perovskite Nanocrystals. *Materials* **2019**, *12*, 3733. [CrossRef]
57. Luo, B.; Naghadeh, S.B.; Zhang, J.Z. Lead Halide Perovskite Nanocrystals: Stability, Surface Passivation, and Structural Control. *ChemNanoMat* **2017**, *3*, 456–465. [CrossRef]
58. Boote, B.W.; Andaraarachchi, H.P.; Rosales, B.A.; Blome-Fernández, R.; Zhu, F.; Reichert, M.D.; Santra, K.; Li, J.; Petrich, J.W.; Vela, J.; et al. Unveiling the Photo- and Thermal-Stability of Cesium Lead Halide Perovskite Nanocrystals. *ChemPhysChem* **2019**, *20*, 2647–2656. [CrossRef]
59. Chen, B.; Wang, S.; Song, Y.; Li, C.; Hao, F. A Critical Review on the Moisture Stability of Halide Perovskite Films and Solar Cells. *Chem. Eng. J.* **2022**, *430*, 132701. [CrossRef]
60. Li, J.; Wang, L.; Yuan, X.; Bo, B.; Li, H.; Zhao, J.; Gao, X. Ultraviolet Light Induced Degradation of Luminescence in CsPbBr3 Perovskite Nanocrystals. *Mater. Res. Bull.* **2018**, *102*, 86–91. [CrossRef]
61. Chatterjee, S.; Biswas, S.; Sourav, S.; Rath, J.; Akhil, S.; Mishra, N. Strategies To Achieve Long-Term Stability in Lead Halide Perovskite Nanocrystals and Its Optoelectronic Applications. *J. Phys. Chem. Lett.* **2024**, *15*, 10118–10137. [CrossRef] [PubMed]
62. Getachew, G.; Huang, W.-W.; Chou, T.-H.; Rasal, A.S.; Chang, J.-Y. Brightly Luminescent (NH4)xCs1-xPbBr3 Quantum Dots for in Vitro Imaging and Efficient Photothermal Ablation Therapy. *J. Colloid Interface Sci.* **2022**, *605*, 500–512. [CrossRef]
63. Cao, Y.; Shao, Y.; Zhang, J.; Chen, C.; Wang, Q. The Photothermal Stability Study of Silica-Coated CsPbBr3 Perovskite Nanocrystals. *J. Solid State Chem.* **2022**, *311*, 123086. [CrossRef]
64. Getachew, G.; Tien, Y.-C.; Kan, T.-C.; Direrssa, W.B.; Wibrianto, A.; Orchirbat, S.; Chang, J.; Rasal, A.S.; Gurav, V.; Kizhepat, S.; et al. Defect-Passivated Metal Halide Perovskite Quantum Dots Stabilized into Biodegradable Porous Polydopamine Nanoparticles for Photothermal/Chemodynamic/Gas Therapy of Cancer. *Chem. Eng. J.* **2023**, *467*, 143560. [CrossRef]
65. Zheng, X.; Hou, Y.; Sun, H.-T.; Mohammed, O.F.; Sargent, E.H.; Bakr, O.M. Reducing Defects in Halide Perovskite Nanocrystals for Light-Emitting Applications. *J. Phys. Chem. Lett.* **2019**, *10*, 2629–2640. [CrossRef]
66. Ye, J.; Byranvand, M.M.; Martínez, C.O.; Hoye, R.L.Z.; Saliba, M.; Polavarapu, L. Defect Passivation in Lead-Halide Perovskite Nanocrystals and Thin Films: Toward Efficient LEDs and Solar Cells. *Angew. Chem.* **2021**, *133*, 21804–21828. [CrossRef]
67. Jellicoe, T.C.; Richter, J.M.; Glass, H.F.J.; Tabachnyk, M.; Brady, R.; Dutton, S.E.; Rao, A.; Friend, R.H.; Credgington, D.; Greenham, N.C.; et al. Synthesis and Optical Properties of Lead-Free Cesium Tin Halide Perovskite Nanocrystals. *J. Am. Chem. Soc.* **2016**, *138*, 2941–2944. [CrossRef]
68. Chen, L.-J.; Lee, C.-R.; Chuang, Y.-J.; Wu, Z.-H.; Chen, C. Synthesis and Optical Properties of Lead-Free Cesium Tin Halide Perovskite Quantum Rods with High-Performance Solar Cell Application. *J. Phys. Chem. Lett.* **2016**, *7*, 5028–5035. [CrossRef]
69. Liu, T.; Zhao, X.; Li, J.; Liu, Z.; Liscio, F.; Milita, S.; Schroeder, B.C.; Fenwick, O. Enhanced Control of Self-Doping in Halide Perovskites for Improved Thermoelectric Performance. *Nat. Commun.* **2019**, *10*, 5750. [CrossRef]
70. Zhong, Q.; Cao, M.; Zhang, Q. Encapsulation of Lead Halide Perovskite Nanocrystals (NCs) at the Single-Particle Level: Strategies and Properties. *Nanoscale* **2021**, *13*, 19341–19351. [CrossRef]
71. Lv, W.; Li, L.; Xu, M.; Hong, J.; Tang, X.; Xu, L.; Wu, Y.; Zhu, R.; Chen, R.; Huang, W. Improving the Stability of Metal Halide Perovskite Quantum Dots by Encapsulation. *Adv. Mater.* **2019**, *31*, 1900682. [CrossRef] [PubMed]
72. Kitazawa, N. Preparation and Optical Properties of Nanocrystalline $(C_6H_5C_2H_4NH_3)_2PbI_4$-Doped PMMA Films. *J. Mater. Sci.* **1998**, *33*, 1441–1444. [CrossRef]

73. Papavassiliou, G.C.; Patsis, A.P.; Lagouvardos, D.J.; Koutselas, I.B. Spectroscopic studies of $(C_{10}H_{21}NH_3)_2PbI_4$,$(CH_3NH_3)(C_{10}H_{21}NH_3)2Pb_2I_7$,$(CH_3NH_3)PbI_3$, and similar compounds. *Synth. Met.* **1993**, *57*, 3889–3894. [CrossRef]
74. Li, S.; Lei, D.; Ren, W.; Guo, X.; Wu, S.; Zhu, Y.; Rogach, A.L.; Chhowalla, M.; Jen, A.K.-Y. Water-Resistant Perovskite Nanodots Enable Robust Two-Photon Lasing in Aqueous Environment. *Nat. Commun.* **2020**, *11*, 1192. [CrossRef] [PubMed]
75. Huang, S.; Li, Z.; Kong, L.; Zhu, N.; Shan, A.; Li, L. Enhancing the Stability of CH_3 NH_3 $PbBr_3$ Quantum Dots by Embedding in Silica Spheres Derived from Tetramethyl Orthosilicate in "Waterless" Toluene. *J. Am. Chem. Soc.* **2016**, *138*, 5749–5752. [CrossRef]
76. Zheng, J.; Zhang, W.; Huang, Y.; Shao, J.; Khan, M.S.; Chi, Y. Encapsulation of Pure Water-Stable Perovskite Nanocrystals (PNCs) into Biological Environment-Stable PNCs for Cell Imaging. *Inorg. Chem.* **2024**, *63*, 5623–5633. [CrossRef]
77. Dirin, D.N.; Benin, B.M.; Yakunin, S.; Krumeich, F.; Raino, G.; Frison, R.; Kovalenko, M.V. Microcarrier-Assisted Inorganic Shelling of Lead Halide Perovskite Nanocrystals. *ACS Nano* **2019**, *13*, 11642–11652. [CrossRef]
78. Jia, X.; Shi, T.; Zhang, Q.; Huang, H.; Chu, P.K.; Yu, X.-F.; He, R. Perovskite Nanocrystals Photo-Initiated in Situ Encapsulation for Optical Tracking. *Chem. Eng. J.* **2024**, *500*, 156756. [CrossRef]
79. Zhang, H.; Wang, X.; Liao, Q.; Xu, Z.; Li, H.; Zheng, L.; Fu, H. Embedding Perovskite Nanocrystals into a Polymer Matrix for Tunable Luminescence Probes in Cell Imaging. *Adv. Funct. Mater.* **2017**, *27*, 1604382. [CrossRef]
80. Talianov, P.M.; Yakubova, A.A.; Bukreeva, A.; Masharin, M.; Eliseev, I.E.; Zelenkov, L.; Muslimov, A.R.; Bukatin, A.; Gordeeva, A.; Kudryavtseva, V.; et al. Incorporation of Perovskite Nanocrystals into Polymer Matrix for Enhanced Stability in Biological Media: In Vitro and In Vivo Studies. *ACS Appl. Bio Mater.* **2022**, *5*, 2411–2420. [CrossRef]
81. Chen, B.; Wang, F. Emerging Frontiers of Upconversion Nanoparticles. *Trends Chem.* **2020**, *2*, 427–439. [CrossRef]
82. Wang, F.; Banerjee, D.; Liu, Y.; Chen, X.; Liu, X. Upconversion Nanoparticles in Biological Labeling, Imaging, and Therapy. *The Analyst* **2010**, *135*, 1839. [CrossRef] [PubMed]
83. Wen, S.; Zhou, J.; Zheng, K.; Bednarkiewicz, A.; Liu, X.; Jin, D. Advances in Highly Doped Upconversion Nanoparticles. *Nat. Commun.* **2018**, *9*, 2415. [CrossRef] [PubMed]
84. He, Y.; Zhang, L.; Chen, G.; Liu, Y.; Shi, S.; Jiang, P.; Ding, J.; Xu, S.; Geng, C. ZnO/SiO_2 Encapsulation of Perovskite Nanocrystals for Efficient and Stable Light-Emitting Diodes. *Appl. Surf. Sci.* **2023**, *611*, 155724. [CrossRef]
85. Miao, Y.; Xie, R.; Kan, Q.; Yu, Y.; Dong, S.; Wang, S.; Mao, L. Silica-Stabilized Lead Halide Perovskite Nanocrystals: Advantages, Progress, and Future Directions. *Adv. Opt. Mater.* **2024**, *13*, 2402320. [CrossRef]
86. Lou, S.; Zhou, Z.; Xuan, T.; Li, H.; Jiao, J.; Zhang, H.; Gautier, R.; Wang, J. Chemical Transformation of Lead Halide Perovskite into Insoluble, Less Cytotoxic, and Brightly Luminescent $CsPbBr_3$ /$CsPb_2$ Br_5 Composite Nanocrystals for Cell Imaging. *ACS Appl. Mater. Interfaces* **2019**, *11*, 24241–24246. [CrossRef]
87. Wei, Y.; Deng, X.; Xie, Z.; Cai, X.; Liang, S.; Ma, P.; Hou, Z.; Cheng, Z.; Lin, J. Enhancing the Stability of Perovskite Quantum Dots by Encapsulation in Crosslinked Polystyrene Beads via a Swelling–Shrinking Strategy toward Superior Water Resistance. *Adv. Funct. Mater.* **2017**, *27*, 1703535. [CrossRef]
88. Kim, Y.-H.; Kim, S.; Kakekhani, A.; Park, J.; Park, J.; Lee, Y.-H.; Xu, H.; Nagane, S.; Wexler, R.B.; Kim, D.-H.; et al. Comprehensive Defect Suppression in Perovskite Nanocrystals for High-Efficiency Light-Emitting Diodes. *Nat. Photonics* **2021**, *15*, 148–155. [CrossRef]
89. Seth, S.; Ahmed, T.; De, A.; Samanta, A. Tackling the Defects, Stability, and Photoluminescence of $CsPbX_3$ Perovskite Nanocrystals. *ACS Energy Lett.* **2019**, *4*, 1610–1618. [CrossRef]
90. Ten Brinck, S.; Zaccaria, F.; Infante, I. Defects in Lead Halide Perovskite Nanocrystals: Analogies and (Many) Differences with the Bulk. *ACS Energy Lett.* **2019**, *4*, 2739–2747. [CrossRef]
91. Avugadda, S.K.; Castelli, A.; Dhanabalan, B.; Fernandez, T.; Silvestri, N.; Collantes, C.; Baranov, D.; Imran, M.; Manna, L.; Pellegrino, T.; et al. Highly Emitting Perovskite Nanocrystals with 2-Year Stability in Water through an Automated Polymer Encapsulation for Bioimaging. *ACS Nano* **2022**, *16*, 13657–13666. [CrossRef] [PubMed]
92. Tedetti, M.; Sempéré, R. Penetration of Ultraviolet Radiation in the Marine Environment. A Review. *Photochem. Photobiol.* **2006**, *82*, 389–397. [CrossRef] [PubMed]
93. Bucci, P.; Prieto, M.J.; Milla, L.; Calienni, M.N.; Martinez, L.; Rivarola, V.; Alonso, S.; Montanari, J. Skin Penetration and UV-damage Prevention by Nanoberries. *J. Cosmet. Dermatol.* **2018**, *17*, 889–899. [CrossRef] [PubMed]
94. Kim, F.H.; Penumadu, D.; Kardjilov, N.; Manke, I. High-Resolution X-Ray and Neutron Computed Tomography of Partially Saturated Granular Materials Subjected to Projectile Penetration. *Int. J. Impact Eng.* **2016**, *89*, 72–82. [CrossRef]
95. Villarraga-Gómez, H.; Morse, E.P.; Smith, S.T. Assessing the Effect of Penetration Length Variations on Dimensional Measurements with X-Ray Computed Tomography. *Precis. Eng.* **2023**, *79*, 146–163. [CrossRef]
96. Slavíková, M.; Krejčí, F.; Žemlička, J.; Pech, M.; Kotlík, P.; Jakůbek, J. X-Ray Radiography and Tomography for Monitoring the Penetration Depth of Consolidants in Opuka—The Building Stone of Prague Monuments. *J. Cult. Herit.* **2012**, *13*, 357–364. [CrossRef]
97. Hao, S.; Daemi, S.R.; Heenan, T.M.M.; Du, W.; Tan, C.; Storm, M.; Rau, C.; Brett, D.J.L.; Shearing, P.R. Tracking Lithium Penetration in Solid Electrolytes in 3D by In-Situ Synchrotron X-Ray Computed Tomography. *Nano Energy* **2021**, *82*, 105744. [CrossRef]

98. Bjärngard, B.E.; Shackford, H. Attenuation in High-Energy X-Ray Beams. *Med. Phys.* **1994**, *21*, 1069–1073. [CrossRef]
99. Archer, B.R.; Fewell, T.R.; Conway, B.J.; Quinn, P.W. Attenuation Properties of Diagnostic X-ray Shielding Materials. *Med. Phys.* **1994**, *21*, 1499–1507. [CrossRef]
100. Ryu, I.; Ryu, J.; Choe, G.; Kwon, H.; Park, H.; Cho, Y.; Du, R.; Yim, S. In Vivo Plain X-Ray Imaging of Cancer Using Perovskite Quantum Dot Scintillators. *Adv. Funct. Mater.* **2021**, *31*, 2102334. [CrossRef]
101. Tseng, W.W.; Winer, D.; Kenkel, J.A.; Choi, O.; Shain, A.H.; Pollack, J.R.; French, R.; Lowy, A.M.; Engleman, E.G. Development of an Orthotopic Model of Invasive Pancreatic Cancer in an Immunocompetent Murine Host. *Clin. Cancer Res.* **2010**, *16*, 3684–3695. [CrossRef]
102. Kim, M.P.; Evans, D.B.; Wang, H.; Abbruzzese, J.L.; Fleming, J.B.; Gallick, G.E. Generation of Orthotopic and Heterotopic Human Pancreatic Cancer Xenografts in Immunodeficient Mice. *Nat. Protoc.* **2009**, *4*, 1670–1680. [CrossRef] [PubMed]
103. Hoffman, R.M. Orthotopic Metastatic Mouse Models for Anticancer Drug Discovery and Evaluation: A Bridge to the Clinic. *Investig. New Drugs* **1999**, *17*, 343–360. [CrossRef] [PubMed]
104. Provenzano, P.P.; Cuevas, C.; Chang, A.E.; Goel, V.K.; Von Hoff, D.D.; Hingorani, S.R. Enzymatic Targeting of the Stroma Ablates Physical Barriers to Treatment of Pancreatic Ductal Adenocarcinoma. *Cancer Cell* **2012**, *21*, 418–429. [CrossRef] [PubMed]
105. Brix, G.; Nissen-Meyer, S.; Lechel, U.; Nissen-Meyer, J.; Griebel, J.; Nekolla, E.A.; Becker, C.; Reiser, M. Radiation Exposures of Cancer Patients from Medical X-Rays: How Relevant Are They for Individual Patients and Population Exposure? *Eur. J. Radiol.* **2009**, *72*, 342–347. [CrossRef] [PubMed]
106. Damilakis, J.; Adams, J.E.; Guglielmi, G.; Link, T.M. Radiation Exposure in X-Ray-Based Imaging Techniques Used in Osteoporosis. *Eur. Radiol.* **2010**, *20*, 2707–2714. [CrossRef] [PubMed]
107. Knight, S.P. A Paediatric X-Ray Exposure Chart. *J. Med. Radiat. Sci.* **2014**, *61*, 191–201. [CrossRef]
108. Hwang, S.-Y.; Choi, E.-S.; Kim, Y.-S.; Gim, B.-E.; Ha, M.; Kim, H.-Y. Health Effects from Exposure to Dental Diagnostic X-Ray. *Environ. Health Toxicol.* **2018**, *33*, e2018017. [CrossRef]
109. Lammertyn, J.; Peirs, A.; De Baerdemaeker, J.; Nicolaı, B. Light Penetration Properties of NIR Radiation in Fruit with Respect to Non-Destructive Quality Assessment. *Postharvest Biol. Technol.* **2000**, *18*, 121–132. [CrossRef]
110. Xiong, X.; Xu, Z.; Huang, H.; Wang, Y.; Zhao, J.; Guo, X.; Zhou, S. A NIR Light Triggered Disintegratable Nanoplatform for Enhanced Penetration and Chemotherapy in Deep Tumor Tissues. *Biomaterials* **2020**, *245*, 119840. [CrossRef]
111. Sun, A.; Guo, H.; Gan, Q.; Yang, L.; Liu, Q.; Xi, L. Evaluation of Visible NIR-I and NIR-II Light Penetration for Photoacoustic Imaging in Rat Organs. *Opt. Express* **2020**, *28*, 9002. [CrossRef] [PubMed]
112. Xu, W.; Wang, D.; Tang, B.Z. NIR-II AIEgens: A Win–Win Integration towards Bioapplications. *Angew. Chem. Int. Ed.* **2021**, *60*, 7476–7487. [CrossRef] [PubMed]
113. Shaw, P.A.; Forsyth, E.; Haseeb, F.; Yang, S.; Bradley, M.; Klausen, M. Two-Photon Absorption: An Open Door to the NIR-II Biological Window? *Front. Chem.* **2022**, *10*, 921354. [CrossRef]
114. Cao, J.; Zhu, B.; Zheng, K.; He, S.; Meng, L.; Song, J.; Yang, H. Recent Progress in NIR-II Contrast Agent for Biological Imaging. *Front. Bioeng. Biotechnol.* **2020**, *7*, 487. [CrossRef]
115. Yao, S.; Belfield, K.D. Two-Photon Fluorescent Probes for Bioimaging. *Eur. J. Org. Chem.* **2012**, *2012*, 3199–3217. [CrossRef]
116. Bestvater, F.; Spiess, E.; Stobrawa, G.; Hacker, M.; Feurer, T.; Porwol, T.; Berchner-Pfannschmidt, U.; Wotzlaw, C.; Acker, H. Two-photon Fluorescence Absorption and Emission Spectra of Dyes Relevant for Cell Imaging. *J. Microsc.* **2002**, *208*, 108–115. [CrossRef]
117. Jethva, P.; Momin, M.; Khan, T.; Omri, A. Lanthanide-Doped Upconversion Luminescent Nanoparticles—Evolving Role in Bioimaging, Biosensing, and Drug Delivery. *Materials* **2022**, *15*, 2374. [CrossRef]
118. Yi, Z.; Luo, Z.; Qin, X.; Chen, Q.; Liu, X. Lanthanide-Activated Nanoparticles: A Toolbox for Bioimaging, Therapeutics, and Neuromodulation. *Acc. Chem. Res.* **2020**, *53*, 2692–2704. [CrossRef]
119. Ma, Q.; Wang, J.; Li, Z.; Lv, X.; Liang, L.; Yuan, Q. Recent Progress in Time-Resolved Biosensing and Bioimaging Based on Lanthanide-Doped Nanoparticles. *Small* **2019**, *15*, 1804969. [CrossRef]
120. Zheng, W.; Huang, P.; Gong, Z.; Tu, D.; Xu, J.; Zou, Q.; Li, R.; You, W.; Bünzli, J.-C.G.; Chen, X. Near-Infrared-Triggered Photon Upconversion Tuning in All-Inorganic Cesium Lead Halide Perovskite Quantum Dots. *Nat. Commun.* **2018**, *9*, 3462. [CrossRef]
121. Liang, T.; Fu, J.; Li, M.; Li, H.; Hao, Y.; Ma, W. Application of Upconversion Photoluminescent Materials in Perovskite Solar Cells: Opportunities and Challenges. *Mater. Today Energy* **2021**, *21*, 100740. [CrossRef]
122. Ruan, L.; Zhang, Y. NIR-Excitable Heterostructured Upconversion Perovskite Nanodots with Improved Stability. *Nat. Commun.* **2021**, *12*, 219. [CrossRef] [PubMed]
123. Zhong, C.-Y.; Xiao, L.; Zhou, J.; Chen, Z.; Chen, Y.; Liu, Z.-Q.; Zhang, J.Z. Two-Photon Photoluminescence and Bio-Imaging Application of Monodispersed Perovskite-in-Silica Nanocrystals with High Biocompatibility. *Chem. Eng. J.* **2022**, *431*, 134110. [CrossRef]
124. Chan, K.K.; Giovanni, D.; He, H.; Sum, T.C.; Yong, K.-T. Water-Stable All-Inorganic Perovskite Nanocrystals with Nonlinear Optical Properties for Targeted Multiphoton Bioimaging. *ACS Appl. Nano Mater.* **2021**, *4*, 9022–9033. [CrossRef]

125. Talianov, P.M.; Peltek, O.O.; Masharin, M.; Khubezhov, S.; Baranov, M.A.; Drabavičius, A.; Timin, A.S.; Zelenkov, L.E.; Pushkarev, A.P.; Makarov, S.V.; et al. Halide Perovskite Nanocrystals with Enhanced Water Stability for Upconversion Imaging in a Living Cell. *J. Phys. Chem. Lett.* **2021**, *12*, 8991–8998. [CrossRef]
126. Pramanik, A.; Patibandla, S.; Gao, Y.; Gates, K.; Ray, P.C. Water Triggered Synthesis of Highly Stable and Biocompatible 1D Nanowire, 2D Nanoplatelet, and 3D Nanocube $CsPbBr_3$ Perovskites for Multicolor Two-Photon Cell Imaging. *JACS Au* **2021**, *1*, 53–65. [CrossRef]
127. Yin, W.; Li, H.; Chesman, A.S.R.; Tadgell, B.; Scully, A.D.; Wang, M.; Huang, W.; McNeill, C.R.; Wong, W.W.H.; Medhekar, N.V.; et al. Detection of Halomethanes Using Cesium Lead Halide Perovskite Nanocrystals. *ACS Nano* **2021**, *15*, 1454–1464. [CrossRef]
128. Jia, D.; Xu, M.; Mu, S.; Ren, W.; Liu, C. Recent Progress of Perovskite Nanocrystals in Chem/Bio Sensing. *Biosensors* **2022**, *12*, 754. [CrossRef]
129. Kim, J.; John, A.T.; Li, H.; Huang, C.; Chi, Y.; Anandan, P.R.; Murugappan, K.; Tang, J.; Lin, C.; Hu, L.; et al. High-Performance Optoelectronic Gas Sensing Based on All-Inorganic Mixed-Halide Perovskite Nanocrystals with Halide Engineering. *Small Methods* **2024**, *8*, 2300417. [CrossRef]
130. Wang, S.; Wei, Z.; Xu, Q.; Yu, L.; Xiao, Y. Trinity Strategy: Enabling Perovskite as Hydrophilic and Efficient Fluorescent Nanozyme for Constructing Biomarker Reporting Platform. *ACS Nano* **2024**, *18*, 1084–1097. [CrossRef]
131. Temur, E.; Zengin, A.; Boyacı, İ.H.; Dudak, F.C.; Torul, H.; Tamer, U. Attomole Sensitivity of Staphylococcal Enterotoxin B Detection Using an Aptamer-Modified Surface-Enhanced Raman Scattering Probe. *Anal. Chem.* **2012**, *84*, 10600–10606. [CrossRef] [PubMed]
132. Wang, J.; Wu, X.; Wang, C.; Shao, N.; Dong, P.; Xiao, R.; Wang, S. Magnetically Assisted Surface-Enhanced Raman Spectroscopy for the Detection of *Staphylococcus Aureus* Based on Aptamer Recognition. *ACS Appl. Mater. Interfaces* **2015**, *7*, 20919–20929. [CrossRef] [PubMed]
133. Xu, Y.; Shi, L.; Jing, X.; Miao, H.; Zhao, Y. SERS-Active Composites with Au–Ag Janus Nanoparticles/Perovskite in Immunoassays for Staphylococcus Aureus Enterotoxins. *ACS Appl. Mater. Interfaces* **2022**, *14*, 3293–3301. [CrossRef]
134. Zhang, J.; Yuan, Z.; Wang, C.; Liu, L.; Wang, Y.; Guo, Y.; Zhao, G. Aqueous-Phase Dual-Functional Chiral Perovskites for Hydrogen Sulfide (H2S) Detection and Antibacterial Applications in Escherichia Coli. *J. Colloid Interface Sci.* **2024**, *661*, 740–749. [CrossRef]
135. Luo, F.; Li, S.; Cui, L.; Zu, Y.; Chen, Y.; Huang, D.; Weng, Z.; Lin, Z. Biocompatible Perovskite Quantum Dots with Superior Water Resistance Enable Long-Term Monitoring of the H_2 S Level in Vivo. *Nanoscale* **2021**, *13*, 14297–14303. [CrossRef]
136. Li, M.; Zeng, Y.; Qu, X.; Jalalah, M.; Alsareii, S.A.; Li, C.; Harraz, F.A.; Li, G. Biocatalytic $CsPbX_3$ Perovskite Nanocrystals: A Self-Reporting Nanoprobe for Metabolism Analysis. *Small* **2021**, *17*, 2103255. [CrossRef]
137. Fu, L.; Qian, Y.; Zhou, J.; Zheng, L.; Wang, Y. Fluorescence-based Quantitative Platform for Ultrasensitive Food Allergen Detection: From Immunoassays to DNA Sensors. *Compr. Rev. Food Sci. Food Saf.* **2020**, *19*, 3343–3364. [CrossRef]
138. Andrásfalvy, B.K.; Galiñanes, G.L.; Huber, D.; Barbic, M.; Macklin, J.J.; Susumu, K.; Delehanty, J.B.; Huston, A.L.; Makara, J.K.; Medintz, I.L. Quantum Dot–Based Multiphoton Fluorescent Pipettes for Targeted Neuronal Electrophysiology. *Nat. Methods* **2014**, *11*, 1237–1241. [CrossRef]
139. Huang, L.; Liao, T.; Wang, J.; Ao, L.; Su, W.; Hu, J. Brilliant Pitaya-Type Silica Colloids with Central–Radial and High-Density Quantum Dots Incorporation for Ultrasensitive Fluorescence Immunoassays. *Adv. Funct. Mater.* **2018**, *28*, 1705380. [CrossRef]
140. Dong, Y.; Tang, X.; Zhang, Z.; Song, J.; Niu, T.; Shan, D.; Zeng, H. Perovskite Nanocrystal Fluorescence-Linked Immunosorbent Assay Methodology for Sensitive Point-of-Care Biological Test. *Matter* **2020**, *3*, 273–286. [CrossRef]
141. Sauer, M.; Heilemann, M. Single-Molecule Localization Microscopy in Eukaryotes. *Chem. Rev.* **2017**, *117*, 7478–7509. [CrossRef] [PubMed]
142. Lelek, M.; Gyparaki, M.T.; Beliu, G.; Schueder, F.; Griffié, J.; Manley, S.; Jungmann, R.; Sauer, M.; Lakadamyali, M.; Zimmer, C. Single-Molecule Localization Microscopy. *Nat. Rev. Methods Primer* **2021**, *1*, 39. [CrossRef] [PubMed]
143. Jin, D.; Xi, P.; Wang, B.; Zhang, L.; Enderlein, J.; Van Oijen, A.M. Nanoparticles for Super-Resolution Microscopy and Single-Molecule Tracking. *Nat. Methods* **2018**, *15*, 415–423. [CrossRef] [PubMed]
144. Yang, Z.; Zong, S.; Yang, K.; Zhu, K.; Li, N.; Wang, Z.; Cui, Y. Wavelength Tunable Aqueous $CsPbBr_3$ -Based Nanoprobes with Ultrahigh Photostability for Targeted Super-Resolution Bioimaging. *ACS Appl. Mater. Interfaces* **2022**, *14*, 17109–17118. [CrossRef]
145. Mei, L.; Xie, R.; Zhu, S.; Deng, S.; Xu, H.; Fan, X.; Yin, W.; Gu, Z. Neurotoxicity Study of Lead-Based Perovskite Nanoparticles. *Nano Today* **2023**, *50*, 101830. [CrossRef]

Disclaimer/Publisher's Note: The statements, opinions and data contained in all publications are solely those of the individual author(s) and contributor(s) and not of MDPI and/or the editor(s). MDPI and/or the editor(s) disclaim responsibility for any injury to people or property resulting from any ideas, methods, instructions or products referred to in the content.